Sci

MDPI

Article

Multi-Sensor Assessment of the Consistency Between Satellite Land Surface Temperature and In Situ Near-Surface Air Temperature over Malta

David Woollard, Adam Gauci and Alfred Micallef *

Department of Geosciences, Faculty of Science, University of Malta, MSD 2080 Msida, Malta; david.woollard.21@um.edu.mt (D.W.); adam.gauci@um.edu.mt (A.G.)
* Correspondence: alfred.micallef@um.edu.mt

Abstract

This study examines land surface temperature (LST) variability over Malta, a small island in the central Mediterranean, using satellite observations compared with in situ near-surface air temperature (NSAT) measurements. The analysis focuses on the comparison between satellite-derived LST and local atmospheric thermal conditions for urban and rural land cover types. LST data from Landsat-8, MODIS (Terra and Aqua), and Sentinel-3A and 3B were analysed over a six-month period (September 2024 to February 2025). Monthly morning and evening field campaigns were conducted at 19 monitoring sites distributed across the island, during which NSAT, relative humidity, wind speed, and wind direction were recorded. Morning comparisons showed strong correlations between satellite-derived LST and in situ NSAT, i.e., Pearson's correlation coefficient, r, in the range of 0.82–0.85. Landsat-8 exhibited a slight positive bias (+1.04 °C), while MODIS and Sentinel-3 Level-2 products showed negative biases (−3.82 °C and −1.89 °C, respectively). Nighttime comparisons revealed larger negative biases for MODIS (−6.91 °C) and Sentinel-3 (−6.89 °C). After empirical-based harmonisation, these discrepancies were reduced to near-zero mean bias, maintaining strong correlations. Spatial analysis indicated a persistent nocturnal urban heat island (UHI) effect, with urban areas retaining more heat than rural zones. Morning patterns showed seasonal modulation: during late summer and early autumn, rural areas exhibited higher surface temperatures due to sparse vegetation and exposed soils, whereas during cooler months the urban signal became more pronounced as vegetation recovery enhanced rural cooling. Overall, the results demonstrate the usefulness of multi-sensor satellite observations, interpreted alongside ground-based measurements for characterising thermal behaviour in small island environments.

Keywords: land surface temperature; near-surface air temperature; remote sensing; urban heat island

Check for updates

Academic Editor: Richard Müller

Received: 2 December 2025
Revised: 13 March 2026
Accepted: 27 March 2026
Published: 3 April 2026

Copyright: © 2026 by the authors. Licensee MDPI, Basel, Switzerland. This article is an open access article distributed under the terms and conditions of the Creative Commons Attribution (CC BY) license.

1. Introduction, Preliminaries and Key Findings

Understanding the thermal behaviour of the Earth's surface and near-surface atmosphere has become increasingly important in the context of rapid urbanisation, climate change, and the rising frequency of extreme weather events [1,2]. LST is the radiometric "skin" temperature of the Earth's surface, a key parameter in the study of surface energy balance, evapotranspiration, drought monitoring, and the UHI effect [3,4]. LST differs from the NSAT measured at weather stations, since LST is the temperature of the land itself, dependent on the absorption, storage, and release of solar radiation. Furthermore, there is

a substantial difference between the thermal heat capacity of land and air, giving rise to a temperature gradient across the boundary of the two media near the Earth's surface [5,6]. Nevertheless, NSAT is strongly related to LST, and the former can be used as a surrogate for the latter, albeit with caution.

Spatial and temporal variability in LST arises from atmospheric radiative transmission, surface albedo, emissivity, moisture availability, and thermal inertia, creating strong contrasts between land cover types and between urban and rural environments [7,8]. Malta represents a particularly challenging and informative setting for thermal analysis. Malta is a small, highly fragmented island environment with a semi-arid Mediterranean climate, extensive coastline, high urbanisation, and strong seasonal vegetation dynamics, exhibiting distinct thermal heterogeneity. Its geographic position in the Central Mediterranean (refer to Figure 1) further accentuates the combined influence of maritime effects and compact land cover diversity on surface thermal dynamics. Impervious urban materials like asphalt and concrete generally exhibit high thermal inertia and therefore store heat during daytime and release it more slowly at night, sustaining elevated nighttime temperatures [9,10]. Vegetated surfaces, in contrast, often cool more efficiently through evapotranspiration and have different thermal characteristics, although the strength of this cooling depends strongly on seasonal phenology and surface moisture availability [11,12]. In a semi-arid Mediterranean setting, these seasonal changes can alter the apparent urban–rural temperature contrast and, in some cases, reduce or even reverse the expected daytime UHI signal.

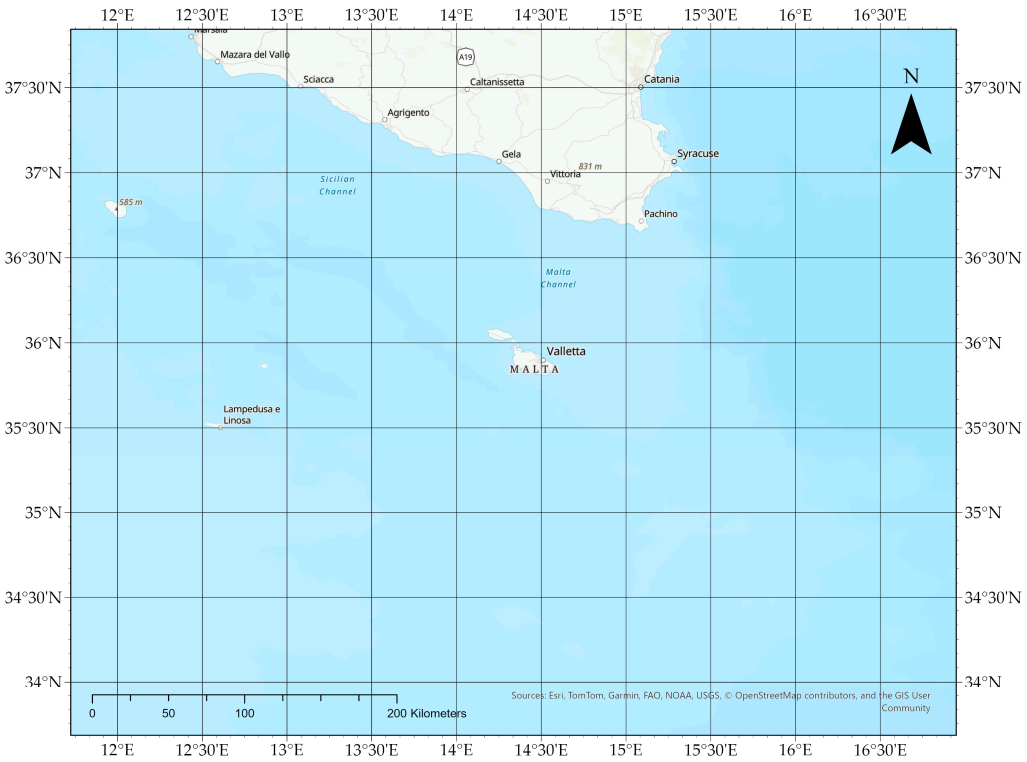


Figure 1. Location of the Maltese Archipelago, in the Central Mediterranean, south of Italy, comprising three islands, namely Malta, Gozo, and Comino. Malta has a Mediterranean climate, characterised by hot, dry summers and mild, wet winters.

Thermal remote sensing exploits the fact that objects with temperatures above absolute zero emit electromagnetic radiation, with peak emission for terrestrial temperatures occurring in the thermal infrared (TIR) region [8,9]. Sensors such as Landsat-8's Thermal Infrared Sensor (TIRS), Sentinel-3's Sea and Land Surface Temperature Radiometer (SLSTR), and the Moderate-Resolution Imaging Spectroradiometer (MODIS) on Terra and Aqua

measure TIR radiance in atmospheric window regions (typically 10–12 μm) that are suitable for LST retrieval [10,13,14]. Converting TIR radiance (or brightness temperature) into LST requires atmospheric and emissivity considerations and is commonly achieved using algorithms such as the split-window approach, which leverages differential absorption between adjacent TIR bands, particularly in the presence of atmospheric water vapour [15–17]. Importantly, sensor design imposes inherent trade-offs. Landsat-8 provides high spatial resolution (30 m) that is well suited to resolving local thermal heterogeneity but has a relatively long revisit cycle (~16 days) and lacks nighttime thermal acquisitions over Malta [10–12]. MODIS provides frequent coverage (typically, daily) but at coarse resolution (~1 km), which can obscure fine-scale urban–rural contrasts [13,18]. Sentinel-3 offers daytime and nighttime observations with moderate spatial resolution in its standard products and also provides Level-1 radiometric data that can be processed to derive LST at improved spatial detail when appropriate retrieval methods are applied [14,19,20]. Essentially, given this stance, the sensors are not capable of directly capturing any daytime–nighttime discrepancy in behaviour and micro-scale UHI structure, and any intercomparison must explicitly account for these constraints.

Retrieval performance depends on environmental context. Previous studies have shown that standard satellite LST products may exhibit systematic deviations due to uncertainties in atmospheric water vapour, surface emissivity, viewing geometry, and sub-pixel heterogeneity, particularly in coastal environments and mixed land–sea settings [21–23].

Several studies have emphasised the importance of local-scale validation using ground-based observations to properly interpret satellite-derived temperatures. For instance, Dyukarev et al. [24] demonstrated the value of in situ measurements for evaluating satellite LST performance under specific environmental conditions, while Ermida et al. [25] highlighted the influence of viewing geometry, illumination angle, and surface heterogeneity on retrieval accuracy.

To improve LST estimation, a variety of correction and modelling approaches have been proposed, including refined physical algorithms, empirical adjustments, and machine-learning-based methods. Wang et al. [26] showed that neural network approaches can enhance LST retrievals under complex atmospheric conditions, while Xu et al. [27] demonstrated that integrating remote sensing data with machine learning can improve the estimation of NSAT. In urban contexts, Lee et al. [28] further illustrated how dynamic land cover changes can significantly alter surface thermal behaviour, underlining the importance of combining satellite observations with in situ measurements when assessing urban–rural thermal contrasts.

In situ observations are particularly important in the case of small islands and coastal zones, where atmospheric moisture and land–sea adjacency can cause standard global algorithms to perform sub-optimally, and where mixed pixels may dominate at kilometre-scale resolution. In this context, in situ observations provide essential constraints for interpreting satellite-derived temperature fields and for evaluating the extent to which satellite LST products are consistent with near-surface thermal conditions.

Despite extensive global research on satellite-based LST, there remains limited locally tailored thermal monitoring work for Malta that systematically evaluates how commonly used satellite products relate to locally observed near-surface thermal conditions across land cover types and seasons [29]. The in situ observations were acquired during six monthly field campaigns spanning September 2024 to February 2025 and include both morning and evening NSAT measurements, as well as relative humidity, wind speed, and wind direction. It should be noted that the in situ campaigns were episodic rather than continuous, and exact temporal coincidence with satellite overpasses was not always achievable. Consequently, satellite observations corresponding to the nearest suitable

clear-sky acquisitions were used, and the analysis is framed as an assessment of consistency and coupling between satellite-derived LST and NSAT under comparable synoptic and seasonal conditions, rather than a strict instantaneous point-to-pixel validation.

The analysis employs mean bias (as a measure of systematic bias), Pearson's correlation coefficient (r), mean squared error (MSE), and paired statistical testing to quantify relationships between datasets across acquisition periods and land cover classes. Lower-resolution sensors in the case of MODIS and Sentinel-3 are interpolated using Inverse Distance Weighting (IDW), with a modified Split-Window Algorithm (SWA) formulated for Sentinel-3 (Level-1 data) to better suit Malta's specific atmospheric and emissivity conditions [17,30]. This enables consistent comparison across sensors while recognising that representativeness error remains unavoidable when comparing point observations to mixed pixels [31]. Additionally, vegetation indices, i.e., Normalized Difference Vegetation Index (NDVI), Normalized Difference Moisture Index (NDMI) [32] and meteorological variables (relative humidity, wind speed, and wind direction) are utilised to examine seasonal and daytime–nighttime thermal patterns [33,34].

Results indicate that whilst Landsat-8 showed the strongest agreement with in situ NSAT measurements during morning acquisitions, its limited revisit frequency and lack of nighttime thermal observations constrained daytime–nighttime analysis. MODIS and Sentinel-3 provide daily morning and nighttime coverage but, at kilometre-scale resolution, tend to smooth local heterogeneity and may exhibit systematic cold biases under humid coastal nighttime conditions [35,36]. To improve the interpretability of Sentinel-3, Level-1 SLSTR observations were processed at 500 m resolution. Since Level-1 data has not undergone atmospheric correction, a SWA was utilised in order to tailor for Malta's specific needs (hereafter referred to as bias-corrected Level-1 data). This adjustment is not presented as a physical correction of 'true' LST; rather, it serves as a harmonisation step that improves consistency with NSAT observations in this case study and highlights the sensitivity of thermal retrievals to local atmospheric conditions [37,38]. This improved agreement with in situ observations.

Another key finding was that while spatial analysis reveals persistent nighttime UHI effects, the daytime UHI was less apparent. It was found that seasonality plays a crucial role, with urban–rural temperature contrasts shifting, depending on background climatic conditions. During warmer months (late summer and early autumn), reduced vegetation cover and elevated rural soil exposure can weaken, mask, or locally reverse the daytime UHI signal, making rural areas appear warmer than urban areas during the morning period. Conversely, in cooler and wetter months, as vegetation cover and surface moisture increase, rural areas cool more efficiently and the expected urban–rural contrast becomes more apparent, particularly during nighttime. Finally, it is emphasised that the observational period covers six months (September to February) and does not include the core summer season; this limits direct inference about peak heat stress conditions and full annual cycle behaviour. Future work should extend observations through summer and, where feasible, incorporate direct in situ radiometric LST measurements to strengthen interpretation of satellite LST products and NSAT coupling in small island environments.

The main contributions of this work are threefold. First, it provides the first structured, Malta-focused intercomparison of widely used satellite LST products with in situ NSAT observations for various land types. Second, it demonstrates a practical, locally tuned processing pathway for Sentinel-3 Level-1 thermal data that improves consistency with near-surface observations in a humid coastal setting. Third, it highlights how seasonal vegetation dynamics in semi-arid Mediterranean islands can modulate, and in morning conditions, occasionally mask, urban–rural thermal contrasts, with implications for small island thermal monitoring and climate adaptation planning.

2. Materials and Methods

This section outlines the approach employed in the study. The research integrates satellite remote sensing data with in situ ground-based measurements to evaluate the consistency and spatial patterns of satellite-derived LST relative to NSAT over Malta, and to understand how different land covers influence the UHI effect on the island.

2.1. Study Area and Sampling Design

Malta is characterised by a semi-arid Mediterranean climate, with hot, dry summers and mild, wet winters. Its small land area (~316 km^2), combined with the varied land cover, ranging from highly urbanised regions to agricultural fields and a substantial coastline, makes Malta a suitable location for examining spatial variability in surface and near-surface thermal conditions.

Nineteen sampling points (listed in Table 1 and graphically shown in Figure 2) were strategically selected across the island. The selection was guided by both practical and scientific considerations, including accessibility, safety, spatial distribution, and the need to represent a range of land cover classes relevant to urban–rural thermal contrasts. The site distribution was chosen so as to provide broad geographic coverage and to capture the main land use types present in Malta. Sampling points 8 to 11 located in Valletta, Sliema and San Ġwann, represent highly urbanised environments and were included to assess anthropogenic influences on near-surface thermal conditions and UHI behaviour. Sampling points 14 to 18 are situated in more rural and agricultural areas of Malta. These allow for a comparison between rural and urban areas, and investigation of the effect of temperature variations. As seen in Figure 2, sampling points 2, 5 and 15 were chosen close to coastal locations to evaluate the potential influence of maritime conditions on local temperature patterns. The coordinates of all sampling points are presented in Table 1. Global Positioning System (GPS) coordinates were recorded for every campaign, i.e., round of in situ measurements, to ensure consistency.

Table 1. List and locations of the 19 sampling points, including the relevant geographical coordinates.

Sampling Point Number	Location by Town/Area	Latitude (°N)	Longitude (°E)	Land Classification
1	Żabbar	35.876955	14.535924	Built-up
2	Żonqor, Marsaskala	35.869689	14.56691	Crop land
3	Marsaskala	35.859617	14.56701	Built-up
4	Żejtun periphery	35.848761	14.54729	Crop land
5	Birżebbuġa	35.826696	14.52732	Built-up
6	Ħal Safi	35.834515	14.50193	Tree cover
7	Luqa	35.859768	14.48863	Built-up
8	Valletta	35.899418	14.51384	Built-up
9	Manoel Island	35.904350	14.4967	Built-up
10	Sliema	35.911289	14.50374	Built-up
11	San Ġwann	35.910797	14.48459	Built-up
12	Mosta	35.910227	14.42546	Built-up
13	Mdina periphery	35.888212	14.40766	Crop land
14	Rabat	35.876516	14.39896	Tree cover
15	Ħad-Dingli	35.860481	14.38184	Built-up

Table 1. *Cont.*

Sampling Point Number	Location by Town/Area	Latitude (°N)	Longitude (°E)	Land Classification
16	Dingli Cliffs	35.857046	14.37376	Grassland
17	Rabat (periphery)	35.903527	14.37717	Tree cover
18	Manikata, Mellieħa	35.950275	14.38508	Grassland
19	Mellieħa (town)	35.961765	14.36021	Built-up

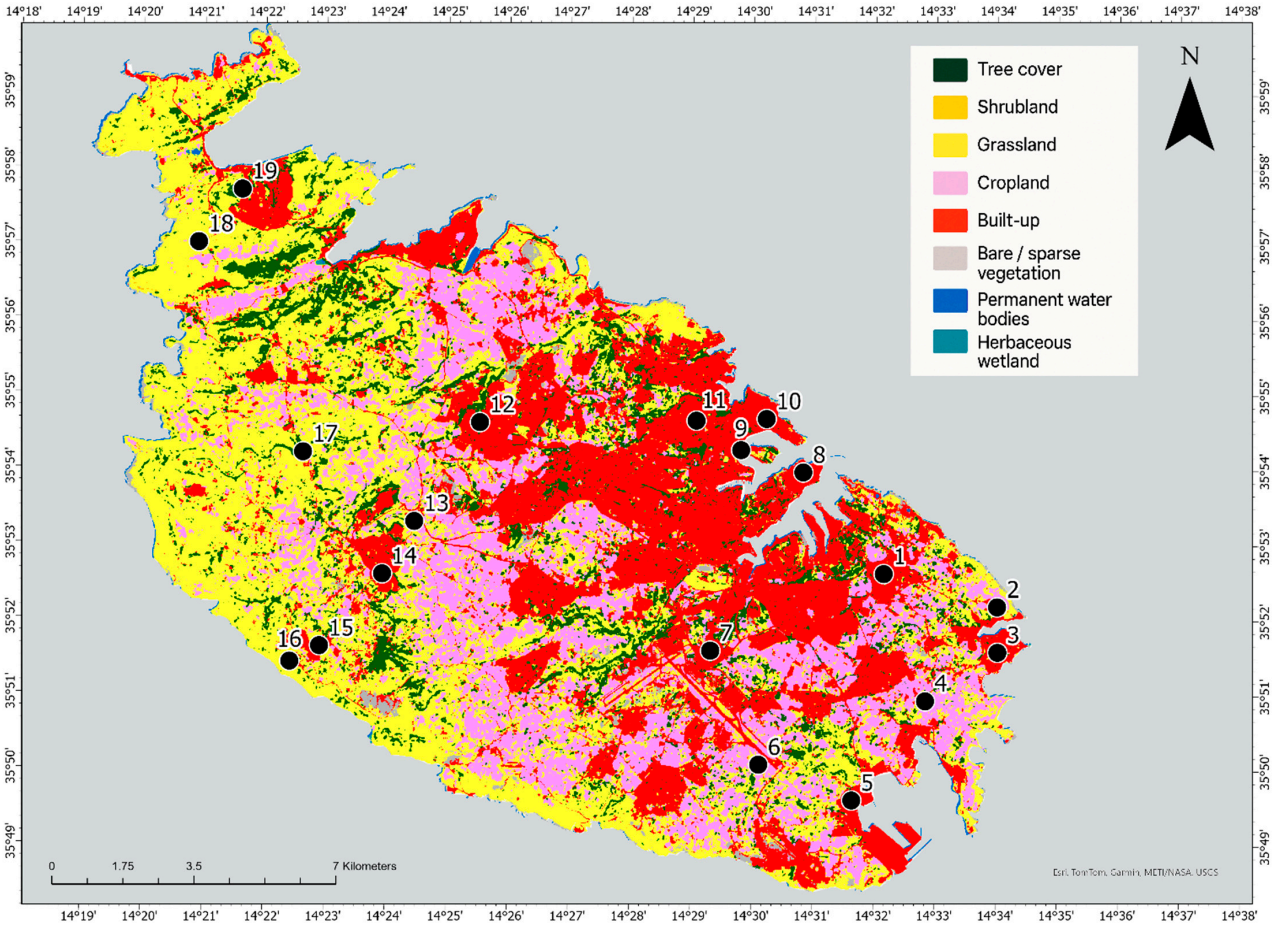


Figure 2. Map of Malta showing the location of the 19 sampling points (black dots) and land type classification (colour-coded).

The land cover classification was based on the European Space Agency (ESA) WorldCover dataset [39], a raster file that represents land cover types at a spatial resolution of 10 m, with an overall accuracy of approximately 75%, as seen in Figure 2. This dataset was used to assign each sampling point to a dominant land cover class and to support subsequent urban–rural comparisons. In situ measurements were conducted in shaded, open areas to ensure that the sensors recorded NSAT conditions without direct solar heating, particularly during morning observations. Sampling points were also selected in relatively open locations, such as squares or gardens, to allow more representative wind measurements and to avoid localised effects such as wind channelling within narrow streets.

Measurements were carried out on a monthly basis from September 2024 to February 2025, resulting in six datasets. Each campaign included both morning (09:00–13:00) and evening (20:00–23:30) observations in order to capture daytime–nighttime temperature contrasts (refer to Table 2). These time windows were chosen to approximate the typical

daytime and nighttime satellite acquisition periods, while remaining compatible with fieldwork logistics and safety constraints. Measurements were always taken at the same geographic coordinates to ensure comparability across campaigns.

Table 2. Dates of the in situ and satellite data acquisition.

Dataset	In Situ Sampling Date	Landsat 8	Sentinel-3	MODIS
1	22/09/2024	06/09/2024	29/09/2024	29/09/2024
2	27/10/2024	16/10/2024	27/10/2024	28/10/2024
3	24/11/2024	25/11/2024	25/11/2024	25/11/2024
4	29/12/2024	11/12/2024	30/12/2024	30/12/2024
5 (only nighttime data collected)	26/01/2025	28/01/2025	28/01/2025	28/01/2025
6	22/02/2025	01/03/2025	02/03/2025	01/03/2025

Data collection was performed only on clear or partly cloudy days to reduce the influence of cloud cover on both in situ and satellite-derived temperature observations. This approach helped to maintain relatively consistent radiative conditions across measurement periods and to minimise cloud-induced biases in temperature and relative humidity readings. Such precautions allowed greater consistency, comparability, and integrity of in situ NSAT and satellite-derived LST measurements. It is acknowledged that point-based in situ measurements cannot fully represent the thermal characteristics of satellite pixels, particularly for coarse-resolution sensors such as MODIS and Sentinel-3. Consequently, the comparisons presented in this study are intended to reflect site-representative or class-scale thermal behaviour rather than exact sampling point-to-pixel equivalence.

2.2. In Situ Measurements

NSAT and relative humidity were measured using a handheld climate data logger by Parkside, model PKDL A1. The instrument has a temperature resolution of 0.1 °C, and an accuracy of ±0.5 °C for temperature (range: −30 to 70 °C). Relative humidity is measured with an accuracy of ±2.5% (range: 0–100%). Wind speed and direction were recorded using the RVM 96B-1 handheld anemometer (by Ames), capable of measuring wind speeds between 0–50 ms^{-1} with a sensitivity of 0.5 ms^{-1} and a directional accuracy of ±2.75° [33,34].

All in situ temperature measurements represent NSAT rather than radiometric LST. Therefore, these measurements were used as a surrogate indicator of local thermal conditions and for assessing the consistency between satellite-derived LST and NSAT.

At each site and during each campaign, three consecutive readings of temperature and relative humidity were recorded and averaged. For wind speed and wind direction, two readings were taken and averaged. This approach was adopted to reduce random measurement error and short-term fluctuations, thereby improving the reliability and consistency of the in situ dataset used for comparison with satellite observations.

2.3. Satellite Data Acquisition and Processing

2.3.1. MODIS

MODIS LST data were obtained from NASA's Application for Extracting and Exploring Analysis Ready Samples (AppEEARS) platform [40]. The analysis utilised Level-2 LST products, provided in raster format at a spatial resolution of approximately 1 km. These products are atmospherically corrected and have undergone radiometric and geometric calibration, reducing uncertainties typically associated with raw Level-1 radiance data.

Both morning (Terra, ~10:30 local time) and nighttime (Aqua, ~01:30 local time) overpasses were included in the analysis to capture daytime–nighttime variations in satellite derived LST, which was then compared to in situ NSAT measurements. Given the coarse spatial resolution of MODIS, individual pixels may contain mixed land cover types and may not fully resolve local thermal heterogeneity across Malta.

To account for the coarse resolution of MODIS and its inability to fully resolve local thermal heterogeneity, IDW interpolation was employed. This ensured that each of the 19 monitoring sites (corresponding to the in situ sampling points) had a representative satellite-derived LST value, enabling direct point-to-pixel comparisons with moderate expectations. The use of atmospherically corrected Level-2 products in combination with IDW interpolation provided spatially continuous temperature fields suitable for comparative analysis across sensors, land cover classes, and observation periods.

2.3.2. Sentinel-3

Sentinel-3 operates as a dual-satellite constellation, i.e., Sentinel-3A and Sentinel-3B, and provides LST data from the SLSTR sensor. To enhance spatial detail beyond the 1 km resolution of the standard Level-2 product, Level-1 Radiometric Brightness Temperature (RBT) data were also processed for the same observation periods. While Level-2 products are atmospherically corrected and directly usable, their coarse resolution often fails to capture the fine-scale thermal heterogeneity of Malta's compact and diverse landscape. To address this, IDW interpolation was applied to the Level-2 datasets, ensuring that each of the 19 monitoring sites was associated with a site-representative LST value. In contrast, Level-1 RBT data were processed using the SWA, producing LST fields at 500 m resolution and offering greater sensitivity to localised thermal contrasts.

The SWA estimates LST using brightness temperatures from the 11 μm (Band 8) and 12 μm (Band 9) channels, with coefficients that account for atmospheric absorption, emissivity, and sensor geometry, using the following formula:

$$\mathrm{LST} = T_8 + a(T_8 - T_9) + b(T_8 - T_9)^2 + c$$

where T_8 and T_9 are brightness temperatures from SLSTR Bands 8 and 9, respectively, and a, b, and c are calibration coefficients [19,22].

The SWA was adopted from established approaches associated with satellite LST retrieval. However, use of the standard coefficients resulted in systematic biases relative to in situ observations, with deviations of several degrees, particularly during nighttime when radiative cooling and elevated relative humidity were pronounced. Of course, these deviations are also due to the fact that the in situ measurements are essentially NSAT and not LST. Nevertheless, irrespective of the latter, such discrepancies are common when working with Level-1 thermal data prior to regional tuning. To address this and the LST-NSAT issue, the SWA coefficients were empirically corrected, or adjusted, using coincident morning and evening in situ measurements, yielding adjusted parameters that more accurately represented the thermodynamic characteristics of Malta's humid coastal environment and this case study. Consequently, the final SWA formulations used in this study were the following:

$$\mathrm{LST}_{\text{Sentinel-Day}} = S_8 + 0.70(S_8 - S_9) + 0.43(S_8 - S_9)^2 - 273.15 + 3$$

$$\mathrm{LST}_{\text{Sentinel-Night}} = S_8 + 0.70(S_8 - S_9) + 0.43(S_8 - S_9)^2 - 273.15 + 9$$

where the brightness temperatures are measured in Kelvin.

The additive terms, +3 °C for daytime and +9 °C for nighttime, were derived from the mean systematic residuals between the Sentinel-3 LST estimates and the corresponding in situ NSAT observations for all stations. For each observation period, the LST-NSAT temperature differences were calculated and aggregated to obtain separate mean biases for daytime and nighttime conditions. These values were then applied as uniform offsets within the modified SWA framework.

This adjustment does not represent a physical recalibration of radiometric LST; rather, it serves as a harmonisation step to improve consistency between satellite-derived LST and NSAT observations for comparative analysis. The larger nighttime offset reflects the stronger cold bias observed under humid coastal conditions, where increased atmospheric water vapour and reduced thermal contrast tend to degrade nighttime thermal retrieval accuracy.

2.3.3. Landsat-8

Landsat-8 data were obtained from the United States Geological Survey (USGS) Earth Explorer portal. For this study, Landsat-8 Collection 2 Level-2 surface temperature data were used. The thermal information is derived from the Thermal Infrared Sensor (TIRS), primarily Band 10 (10.6–11.19 μm). Surface temperature values were converted following the Landsat-8 and Landsat-9 Collection 2 Level-2 Science Product Guide [35]. In this study, LST was calculated using the following expression:

$$\mathrm{LST}_{\text{Landsat-8}} = (S_{B10} \times 0.00341802) + 149 - 273.15$$

where S_{B10} represents the Landsat Level-2 surface temperature digital values from Band 10. Multiplication by the scale factor 0.00341802 and addition of the offset 149.0 convert the digital values to temperature in Kelvin. Subtracting 273.15 converts the values to degrees Celsius, allowing comparison with in situ NSAT.

This procedure yields atmospherically corrected surface temperature values from the Landsat Level-2 product. The higher spatial resolution of Landsat-8 (30 m) is particularly useful for resolving localised thermal variability across Malta's mixed urban and rural environments.

It should be noted that Landsat-8 acquisitions over Malta occur only during daytime overpasses. Consequently, Landsat-8 data were used solely for morning analyses and were not included in daytime–nighttime comparisons. MODIS and Sentinel-3, which provide both daytime and nighttime observations, were used for sub-diurnal comparisons.

2.4. Statistical Analysis

Evaluation of satellite-derived LST relative to in situ observations of NSAT was carried out using a number of statistical metrics. Mean bias was calculated to assess systematic offsets between satellite-derived LST and NSAT measurements. Pearson's correlation coefficient, *r*, quantified the strength and direction of the linear relationship between the datasets, while the mean squared error (MSE) measured the overall magnitude of deviations, giving greater weight to larger differences. In addition, paired two-tailed *t*-tests were applied to evaluate whether differences between satellite-derived and in situ mean temperatures were statistically significant.

All statistical analyses were performed using Python 3.13.0 with NumPy 1.26.4, SciPy 1.17.1, and Pandas 2.3.0. Prior to applying parametric tests, the normality of paired differences was assessed using the Shapiro–Wilk test. Where the normality assumption was satisfied, paired *t*-tests were applied; otherwise, results were interpreted cautiously and compared with non-parametric alternatives (Wilcoxon signed-rank test), which produced consistent conclusions.

The analyses were grouped by time of acquisition (morning and nighttime passes) and by land cover class (urban and rural sites). This allowed the assessment of daytime–nighttime differences in sensor behaviour, as well as the influence of surface characteristics on the relationship between satellite-derived LST and in situ NSAT.

3. Results

3.1. Validation of Satellite-Derived LST Using In Situ Measurements

This sub-section examines the relationship between satellite-derived LST data from Landsat-8, MODIS, and Sentinel-3 by comparing them with ground-based NSAT measurements at the 19 monitoring sites. The analysis focuses on the consistency between LST estimates and NSAT observations, rather than on strict validation of LST accuracy.

3.1.1. Daytime Consistency Between Satellite-Derived LST and In Situ NSAT

Landsat-8, with its 30 m spatial resolution, provided the most detailed LST fields among the examined sensors. Comparison with in situ NSAT measurements showed a slight positive LST-NSAT bias (mean bias = 1.04 °C), as expected since LST tends to be higher than NSAT. Nevertheless, linear correlation was strong (r = 0.83) as displayed in Figure 3a. However, variability was notable (MSE = 48.26 °C), particularly on the warmest acquisition day. This is not surprising given that LST is being compared with NSAT (as surrogate). The paired *t*-test indicated no statistically significant difference between the Landsat-8 LST and the in situ NSAT measurements ($p = 0.146$). This suggests that, under the conditions examined, Landsat-8 LST exhibited strong coupling with NSAT, while still reflecting the inherent physical differences between the two variables.

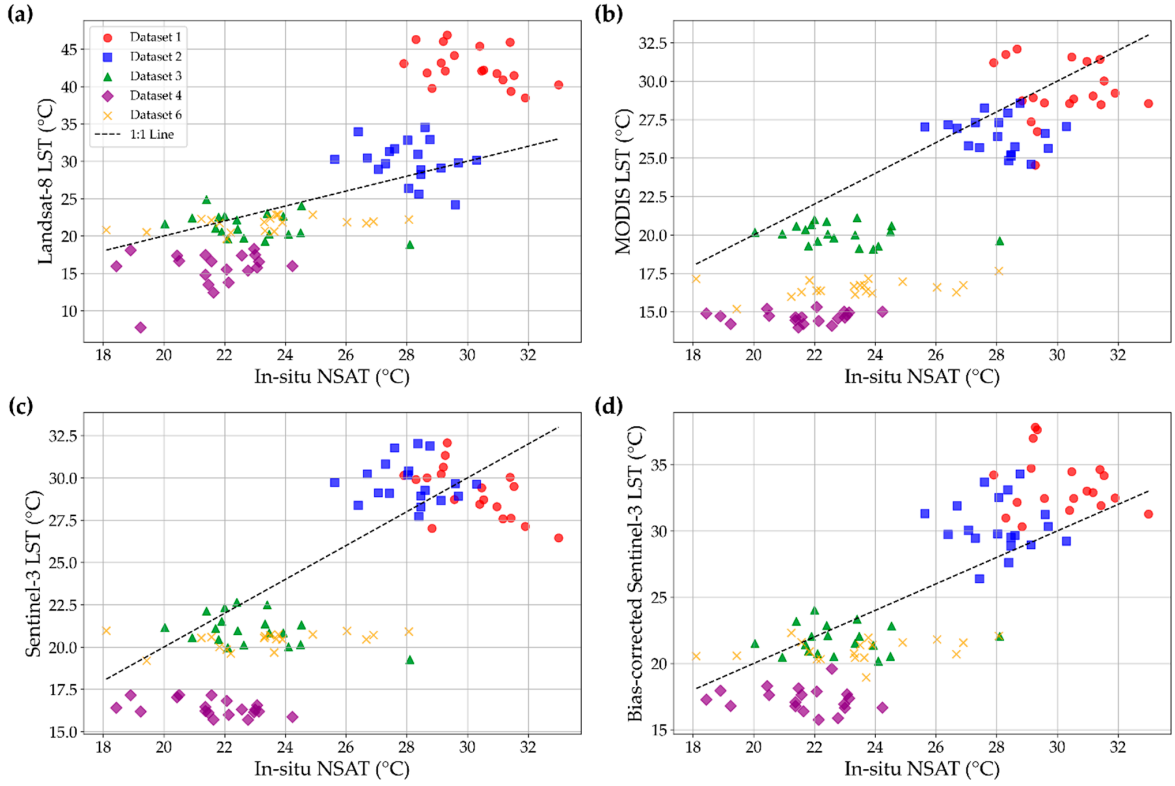


Figure 3. Comparison of morning satellite-derived LST (ordinate) with morning in situ NSAT measurements (abscissa) using five distinct datasets (corresponding to five monitoring campaigns × 19 data points, i.e., n = 95): (**a**) Landsat-8, (**b**) MODIS, (**c**) Sentinel-3, and (**d**) bias-corrected Sentinel-3. The five different datasets are colour-coded for distinction. The dashed 1:1 line indicates perfect agreement, highlighting the bias and spread in each case.

In contrast, MODIS Level-2 products, whose comparison is displayed in Figure 3b, exhibited a systematic negative bias relative to NSAT, with a mean bias of −3.82 °C and MSE of 25.28 °C, although correlation with in situ data remained high (r = 0.85). The underestimation was statistically significant ($p < 0.001$).

This behaviour is primarily attributable to the coarse spatial resolution of MODIS (1 km), which averages over mixed land cover types and smooths fine-scale urban–rural contrasts. To enable comparison with the point-based in situ measurements, IDW interpolation was used to derive site-representative satellite temperature values at the sampling locations. While this improved spatial coherence for comparison purposes, it could not fully resolve abrupt thermal transitions in heterogeneous environments, contributing to persistent differences between MODIS LST and NSAT.

A similar negative bias was observed in Sentinel-3 Level-2 products, which differed from in situ NSAT by −1.89 °C (r = 0.82, MSE = 13.20 °C). The systematic difference ($p < 0.001$) likewise reflects the limitations of kilometre-scale resolution and the smoothing effect associated with mixed land–sea and urban–rural pixels.

To explore the sensitivity of Sentinel-3 retrievals to local conditions, Level-1 RBT data were processed using a regionally adjusted SWA, producing LST fields at 500 m resolution. The corrected dataset, shown in Figure 3d, exhibited a substantially reduced bias relative to NSAT, with a mean bias of −0.44 °C, correlation coefficient of 0.86, and MSE of 13.58 °C. The bias was not statistically significant ($p = 0.250$), indicating improved consistency following the empirical adjustment.

This improvement reflects the effect of the empirical adjustment, which harmonises the satellite-derived LST with NSAT observations under local atmospheric conditions. As discussed previously, this corrected product should be interpreted as a site-consistent temperature estimate rather than a strictly physical representation of radiometric LST.

3.1.2. Nighttime Consistency Between Satellite-Derived LST and In Situ NSAT

Nighttime comparisons revealed larger LST-NSAT biases between satellite-derived LST and in situ NSAT than during daytime conditions, particularly for the coarse-resolution sensors.

As shown in Figure 4a, MODIS exhibited a negative bias relative to NSAT (mean bias = −6.91 °C, r = 0.87, MSE = 52.55 °C), while Sentinel-3 Level-2 data (Figure 4b) showed nearly identical behaviour (mean bias = −6.89 °C, r = 0.75, MSE = 55.09 °C). In both cases, the bias relative to NSAT were statistically significant ($p < 0.001$).

The similarity of these biases suggests that the behaviour is not primarily sensor-specific but is instead related to the limitations of kilometre-scale nighttime thermal retrievals in heterogeneous coastal environments. Mixed pixels, radiative surface cooling, and the smoothing effect associated with IDW interpolation all contribute to systematic differences between satellite-derived surface temperatures and point-based NSAT measurements, which tends to smooth local maxima and minima and exacerbate the cold bias.

Empirical calibration or adjustment of Sentinel-3 Level-1 data using the modified SWA reduced the magnitude of this bias, as shown in Figure 4c. The mean bias relative to NSAT was reduced to +1.31 °C, with the MSE decreasing to 9.61 °C, while correlation remained strong (r = 0.83). Although the bias remained statistically significant ($p < 0.001$), the reduced bias indicates improved consistency between the adjusted satellite-derived LST and in situ NSAT observations under nighttime conditions.

To further examine the systematic negative biases observed in the MODIS and Sentinel-3 nighttime Level-2 products, an empirical adjustment factor of +6.86 °C was applied (Figure 5). This factor was derived from the mean difference between satellite-

derived LST and in situ NSAT across all nighttime datasets and represents the average LST-NSAT bias between the two quantities.

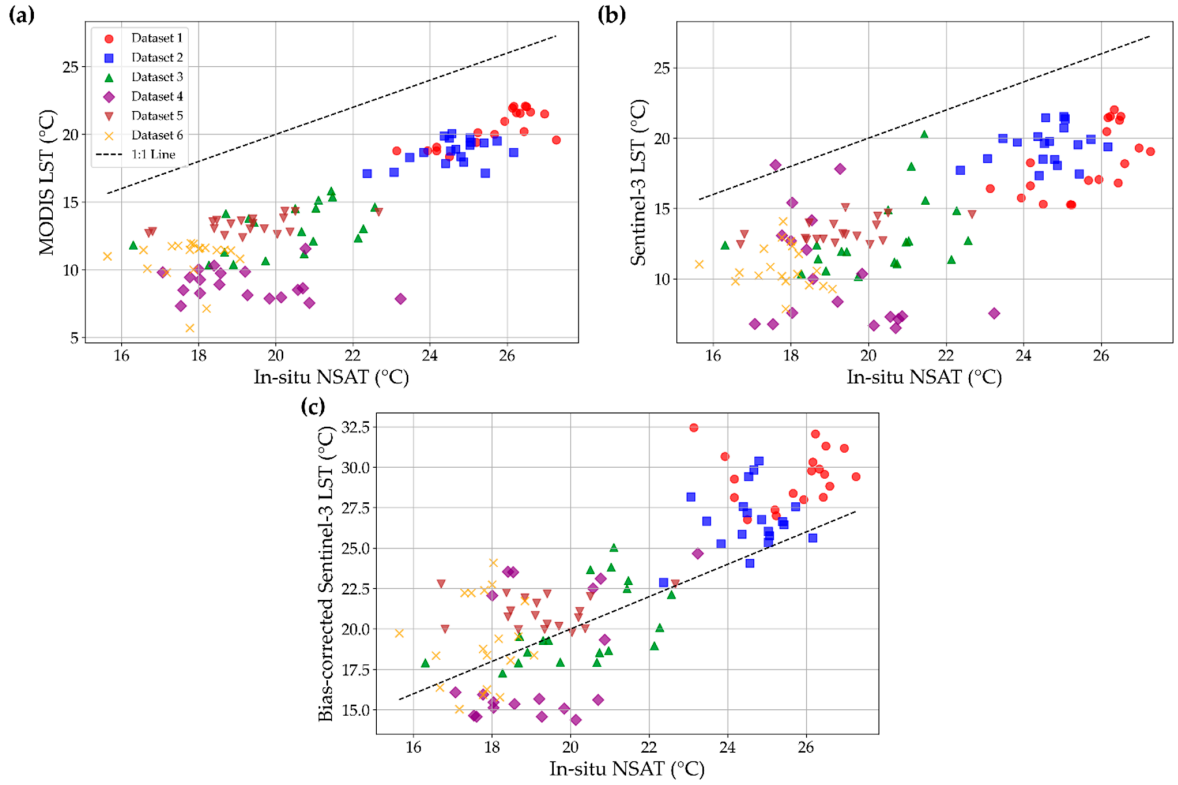


Figure 4. Comparison of nighttime satellite-derived LST (ordinate) with nighttime in situ NSAT measurements (abscissa) using six datasets (corresponding to six monitoring campaigns × 19 data points, i.e., n = 114) for: (**a**) MODIS, (**b**) Sentinel-3, and (**c**) bias-corrected Sentinel-3. The six different datasets are colour-coded for distinction. The dashed 1:1 line indicates perfect agreement, highlighting the bias and spread.

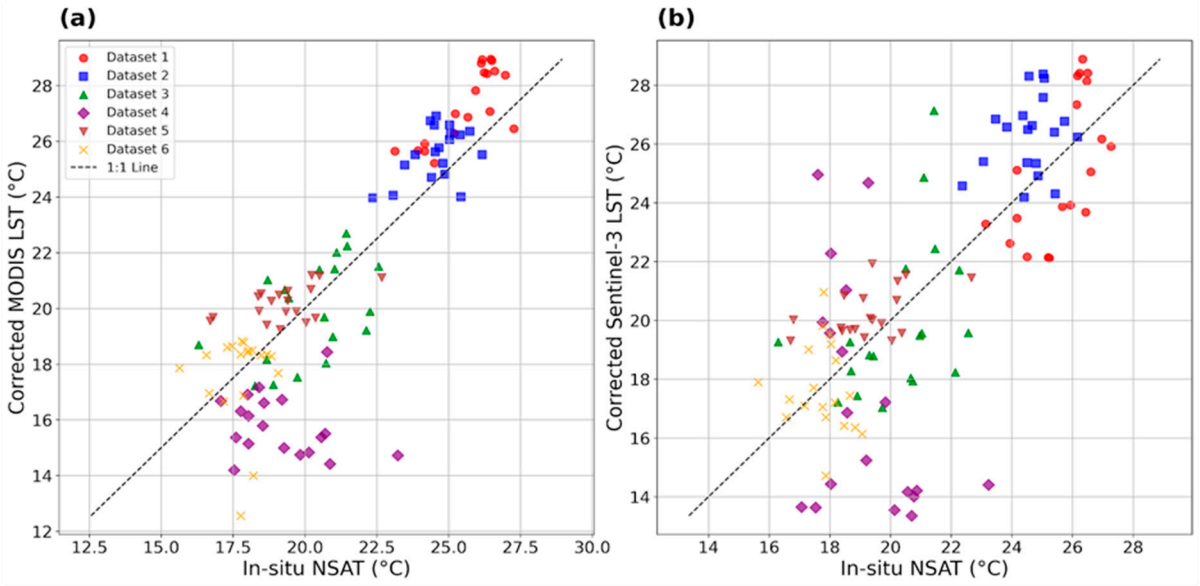


Figure 5. Comparison of nighttime satellite-derived LST from (**a**) MODIS and (**b**) Sentinel-3, with in situ NSAT measurements, using six distinct datasets. A correction factor of +6.86 °C was applied to account for consistent underestimation seen in Figures 4a and 4b, respectively. Both sensors exhibit strong correlation with in situ data (r = 0.87 for MODIS and r = 0.75 for Sentinel-3).

Application of this adjustment reduced the mean bias relative to NSAT to −0.05 °C for MODIS and −0.03 °C for Sentinel-3, with corresponding MSE values of 4.87 °C and 7.58 °C. Following adjustment, no statistically significant differences were detected relative to the in situ measurements (p = 0.828 for MODIS and p = 0.899 for Sentinel-3).

These results indicate that, while the raw Level-2 nighttime products exhibit consistent biases relative to NSAT (used as surrogate for LST), simple empirical harmonisation can substantially improve agreement with NSAT observations for the purposes of site-based or class-scale thermal analysis. As discussed earlier, such adjustments should be interpreted as practical harmonisation steps rather than physical corrections of radiometric LST.

3.2. Influence of Atmospheric Conditions on LST Accuracy

To assess the influence of local atmospheric conditions on the discrepancies between satellite-derived LST and ground-based NSAT, three additional parameters were considered, namely, relative humidity, wind speed, and wind direction. These meteorological factors are known to influence land surface–atmosphere energy exchange and may therefore affect both the in situ measurements and the relationship between satellite-derived LST and NSAT, particularly during transitional morning and evening periods.

Relative humidity emerged as the most consistent and significant factor associated with the LST-NSAT biases, as shown in Figure 6. In the case of the morning, i.e., daytime, datasets (refer to Figure 6a), positive correlations were observed between relative humidity and satellite bias for all three satellites, i.e., Landsat-8 (r = 0.62, $p = 2.39 \times 10^{-11}$), MODIS (r = 0.54, $p = 1.67 \times 10^{-8}$), and Sentinel-3 (r = 0.40, $p = 5.65 \times 10^{-5}$). This indicates that higher atmospheric moisture is associated with larger LST-NSAT biases, particularly in standard LST products that rely on simplified atmospheric corrections.

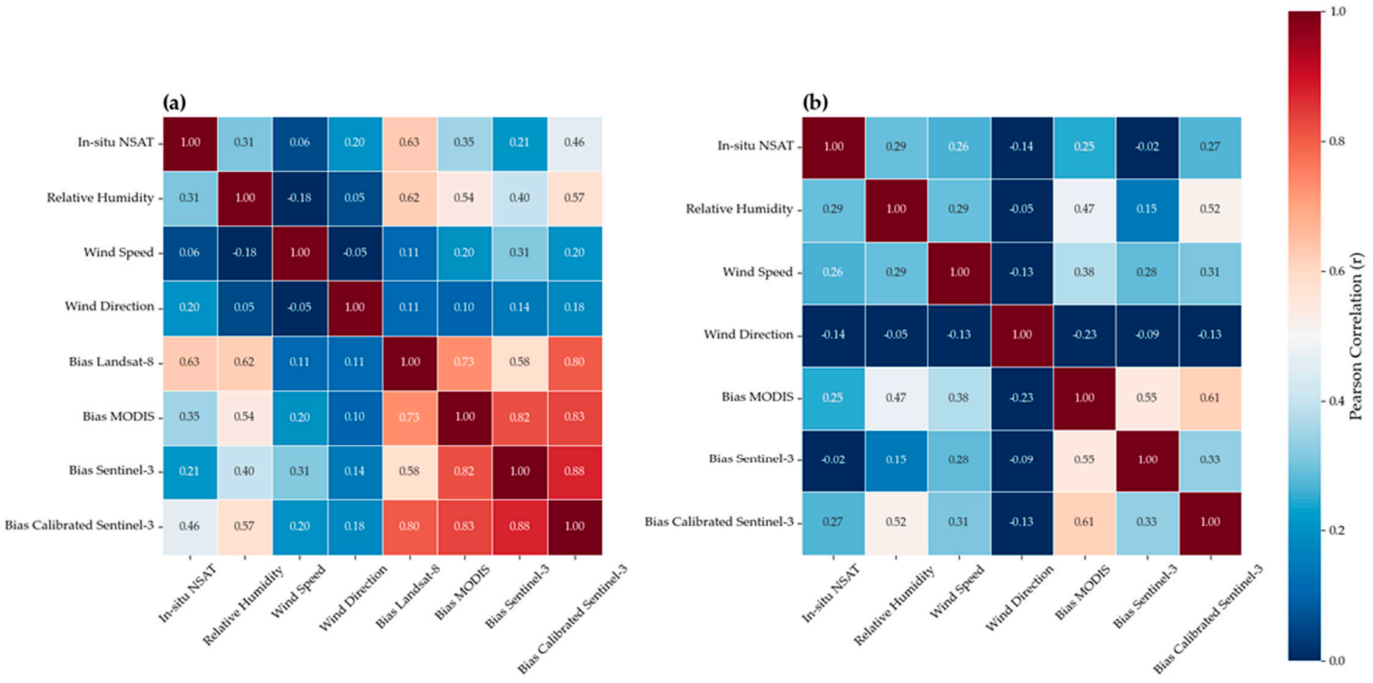


Figure 6. Correlation matrices (as 'heat' maps) showing relationships between in situ measured meteorological data (NSAT, RH, WS, and WD) and satellite biases for (**a**) daytime and (**b**) nighttime datasets. Definition of variables: NSAT—Near-Surface Air Temperature (°C); RH—relative humidity (%); WS—wind speed (ms^{-1}); WD—wind direction (°); Bias Landsat, Bias MODIS, Bias Sentinel—difference between satellite-derived LST and in situ measured NSAT.

For the evening, i.e., nighttime, datasets (refer to Figure 6b), relative humidity continued to show an influence, although correlations were weaker. A significant link was

observed with in situ NSAT measurements (r = 0.29, $p = 1.75 \times 10^{-3}$) and MODIS LST-NSAT bias (r = 0.47, $p = 1.10 \times 10^{-7}$), but the association with Sentinel-3 bias was not significant (r = 0.15, $p = 0.115$). This suggests that the response to atmospheric moisture varies between sensors and retrieval approaches, particularly under nighttime conditions characterised by surface cooling, stratification, and reduced vertical mixing.

The associated mechanism is well established: water vapour strongly absorbs and re-emits longwave radiation in the 10–12 μm atmospheric window, reducing the effective signal reaching the sensor when the relative humidity is high. Without accurate relative humidity parameterisation, this can lead to systematic differences between satellite-derived LST and NSAT, especially in coastal or island environments where relative humidity frequently exceeds 80%. In Malta, this effect is most pronounced during the early morning and post-sunset passes, when land surface–atmosphere disequilibrium is greatest [34]. These findings align with previous work demonstrating the critical role of atmospheric water vapour in relevant satellite retrieval errors [5,24,30].

The effect of wind speed was generally limited compared with that of relative humidity. For the morning datasets, correlation with in situ NSAT measurements was negligible (r = 0.06, $p = 0.581$). A moderate correlation was observed with Sentinel-3 LST-NSAT bias (r = 0.31, $p = 1.95 \times 10^{-3}$) and a weaker association with MODIS (r = 0.20, $p = 0.053$). These results suggest that wind-driven convection plays a secondary role during the morning period, when surface heating is primarily controlled by radiative forcing and local surface properties. Under these conditions, the development of the near-surface temperature field is dominated by solar input, surface moisture availability, and emissivity, while moderate variations in wind speed are less effective at altering the overall land surface–air temperature relationship [41].

For the evening datasets, wind effects became more apparent, with statistically significant correlations observed with in situ NSAT measurements (r = 0.26, $p = 4.47 \times 10^{-3}$), MODIS bias (r = 0.38, $p = 3.40 \times 10^{-5}$), and Sentinel-3 bias (r = 0.28, $p = 2.20 \times 10^{-3}$). This behaviour is consistent with the transition to more stable nocturnal boundary layer conditions, where radiative cooling at the surface leads to temperature stratification. Under such conditions, wind speed influences the degree of turbulent mixing between the surface and the overlying air. Higher wind speeds can enhance vertical mixing, reducing near-surface temperature gradients and moderating the difference between LST and NSAT, whereas calmer conditions promote stronger decoupling and larger temperature contrasts.

Despite these statistically significant nighttime correlations, the overall strength of the explanation concerning wind speed remains lower than that of relative humidity, indicating that atmospheric moisture and longwave radiative processes are the dominant drivers of LST-NSAT discrepancies in this coastal Mediterranean setting. Wind direction, by contrast, exhibited no detectable relationship with the LST-NSAT bias in either the daytime or nighttime datasets. This is likely due to the small spatial scale of Malta and the prevalence of maritime air masses, where sea breeze circulations from different sectors produce broadly similar thermal and humidity conditions, limiting any consistent directional influence on retrieval bias [42].

Together, these results highlight the dominant role of relative humidity in shaping differences between satellite-derived LST and in situ NSAT, particularly in humid coastal environments. Wind speed appears to exert a secondary, stability-dependent influence, while wind direction shows no systematic effect during the observational period.

3.3. Urban vs. Rural LST and the UHI Effect

This sub-section examines differences in thermal behaviour between urban and rural areas across Malta, with particular focus on the UHI effect. By analysing satellite-derived

LST alongside in situ NSAT measurements, the study explores how land cover type, seasonal conditions, and daytime–nighttime contrasts influence observed temperature patterns. The results provide insight into the spatial and temporal variability of urban–rural thermal differences, while recognising the limitations associated with mixed pixels and point-based observations.

3.3.1. Daytime Urban–Rural Thermal Contrasts

As described previously, the sampling locations were distributed across Malta to enable a comparison between built-up and rural settings. Urban–rural class membership was assigned using ESA WorldCover at 10 m resolution, providing a consistent land cover classification and reducing the likelihood of misclassification.

Morning LST from Landsat-8, MODIS, Sentinel-3 Level-2, and the bias-corrected Sentinel-3 SWA product were grouped by land cover class for all observation periods. When data from the six datasets were aggregated, the overall median LST for urban and rural areas appeared broadly similar. However, when examined on a per-dataset basis, more pronounced class-specific differences became evident. During the warmer part of the study period (late summer and early autumn), corresponding to datasets 1 to 3 (September to November), showed that rural areas consistently recorded higher median LST than their urban counterparts, with differences reaching approximately 3 to 4 °C. This pattern was noted for data from all four satellites and is especially clear in the case of MODIS and the bias-corrected Sentinel-3 boxplots (refer to Figure 7), where rural LST distributions exhibit both higher medians and a wider interquartile range (IQR) compared to urban zones.

These LST differences, where rural land surfaces appear warmer than those in urban areas, in the morning, reflects the limited vegetative cover, higher albedo, and lower evapotranspiration rates typical of rural zones during the drier late summer and early autumn months. Exposed soil and rock surfaces in agricultural and semi-rural areas absorb solar radiation more efficiently, causing a rapid increase in surface temperature after sunrise, leading to elevated LST values. In contrast, urban areas, despite their impervious surfaces, are often subject to early morning shadowing effects, complex surface geometry, and higher building reflectivity, e.g., light-coloured roofs, which can moderate surface warming in the immediate post-sunrise period [43,44].

However, this thermal pattern shifts as one progresses to the colder months (datasets 4 to 6, corresponding to December to February). During this period, median rural LST values decrease, while urban values remain comparatively elevated. The boxplots (refer to Figure 7) clearly reflect this transition, with rural medians decreasing by up to 5 °C, while plots for urban areas retain higher medians. This shift corresponds to the restoration of vegetative cover in rural areas, as supported by NDVI and NDMI analyses from Sentinel-2 data and further explained in the following discussion.

To support this interpretation, vegetation and moisture indicators (referring to NDVI and NDMI derived from Sentinel-2) were computed and spatially aggregated over rural classes (refer to Figure 8). Over the study period, NDVI increased from approximately 0.15 to 0.45 and while NDMI rose from roughly −0.10 to 0.20. These trends indicate increasing canopy density and surface moisture, which are associated with enhanced evapotranspirative cooling and reduced rural daytime LST.

These seasonal changes in surface conditions help explain why aggregated statistics for the morning datasets do not always display a pronounced UHI signal, even though class-based differences are evident on individual observation days. It is also important to note that the analysis is based on mixed satellite pixels and point-based in situ measurements; therefore, the observed contrasts should be interpreted as class-scale thermal tendencies rather than strictly localised temperature differences.

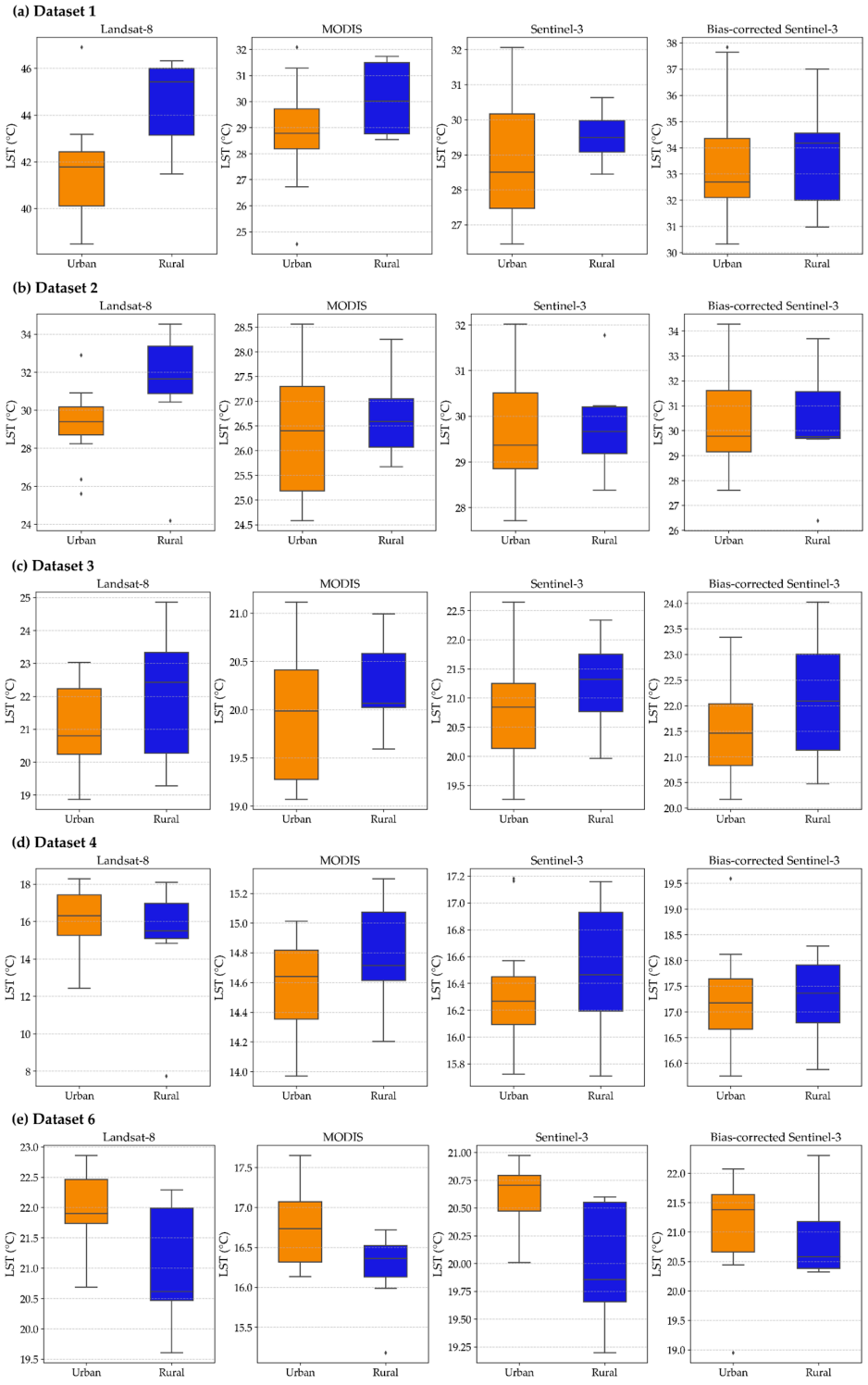


Figure 7. Boxplots illustrating the distribution of satellite-derived LST across urban and rural land use classes for each observation day (datasets 1–6, excluding dataset 5) during the morning acquisition period. Each box represents the IQR, capturing the middle 50% of LST values within each class, while the horizontal line within the box indicates the median temperature. The whiskers extend to 1.5 times the IQR, highlighting the spread. The data outliers are points beyond the whiskers. The figure provides a comparative overview of the LST variability between urban and rural areas over multiple observation days. Higher median LST values in urban areas compared to rural ones generally indicate the presence of an UHI effect, driven by differences in surface properties, such as albedo, thermal inertia, and impervious surface coverage. Variations across the datasets reflect changing meteorological conditions and seasonal influences that modulate the intensity of the temperature contrast between land cover types.

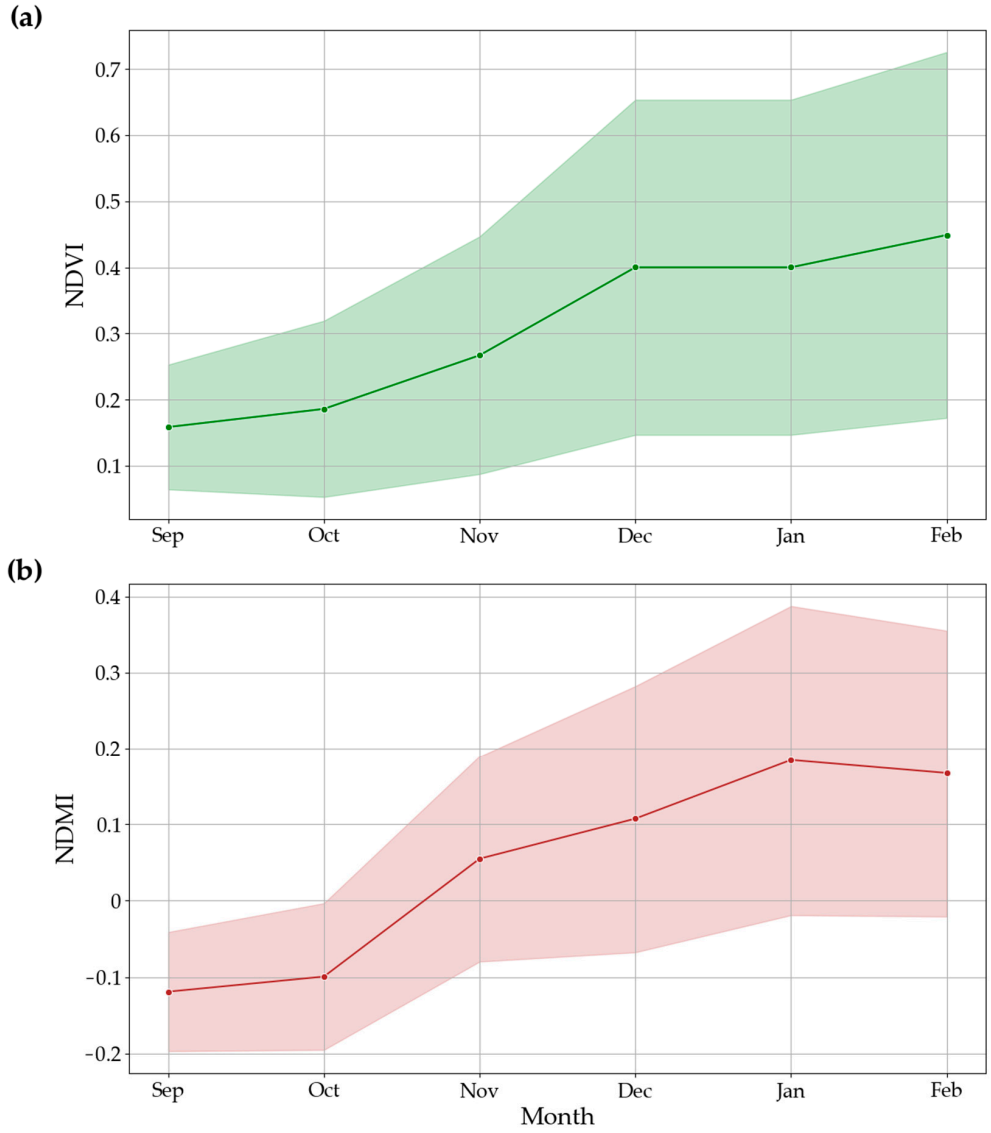


Figure 8. (**a**) NDVI and (**b**) NDMI derived from Sentinel-2 Level-2A surface reflectance imagery for Malta's rural areas. Both indices were computed using spectral bands retrieved from the Copernicus Open Access Hub of the European Space Agency [14], with NDVI calculated as $(\mathrm{NIR} - \mathrm{RED})/(\mathrm{NIR} + \mathrm{RED})$ and NDMI as $(\mathrm{NIR} - \mathrm{SWIR})/(\mathrm{NIR} + \mathrm{SWIR})$, where NIR refers to the Near-Infrared Band (typically, 0.7–1.1 µm), RED is the Red Band (typically, 0.6–0.7 µm), and SWIR is the Short-wave Infrared Band (typically, 0.9–2.5 µm). Note that, NDVI provides a quantitative measure of vegetation greenness and canopy density, while NDMI indicates relative surface moisture content and vegetation water stress. The spatial patterns highlight the contrast between densely vegetated and built-up or sparsely vegetated areas, with higher NDVI and NDMI values corresponding to healthy, moisture-rich vegetation.

Landsat-8 exhibited the greatest ability to resolve intra-urban temperature differences and delineate microclimatic variations within the built environment, owing to its higher spatial resolution. For instance, in dataset 6 (refer to Figure 7), Landsat-8 recorded a distinct urban–rural LST contrast of nearly 1.3 °C, with urban areas averaging 22.0 °C and rural areas 20.6 °C. This difference is consistent with the expected UHI behaviour and reflects the capability of high-resolution imagery that effectively distinguishes impervious surfaces, shading effects, and localised land cover heterogeneity within urban areas.

In contrast, MODIS and Sentinel-3 Level-2 products were more limited in resolving fine-scale temperature differences. Nevertheless, both sensors still reflected broader-scale

urban–rural contrasts, particularly during the cooler months when vegetation recovery enhanced rural cooling. MODIS recorded a difference of approximately 0.5 °C between urban (16.8 °C) and rural (16.3 °C) areas, while Sentinel-3 Level-2 showed a 0.7 °C difference (urban: 20.6 °C and rural: 19.9 °C). These results indicate that even coarser-resolution satellite sensors can reveal key features of the UHI effect, especially when seasonal conditions heighten temperature differences between land cover types.

The bias-corrected Sentinel-3 SWA product, with an effective spatial resolution of 500 m, provided an intermediate representation between spatial detail and temporal frequency. In this case, by processing Level-1 data with a locally adjusted SWA rather than relying solely on interpolated Level-2 products, the dataset preserved more of the original spatial variability and enabled clearer identification of subtle thermal contrasts. In dataset 4, the bias-corrected Sentinel-3 showed a modest but consistent urban–rural difference of 0.2 °C (urban: 17.2 °C and rural: 17.4 °C). Although the magnitude of this difference was smaller than that observed in Landsat-8, the result reflects the expected smoothing associated with moderate spatial resolution and the harmonisation of LST with NSAT-based observations.

These results illustrate the practical trade-off in satellite-based UHI analysis. Higher-resolution platforms such as Landsat-8 capture stronger localised thermal contrasts but are limited by lower temporal frequency, whereas coarser sensors such as MODIS and Sentinel-3 provide more frequent coverage but at the cost of spatial detail. The bias-corrected Sentinel-3 SWA dataset represents a useful intermediate approach, particularly for small island contexts such as Malta, where both spatial detail and revisit frequency are important.

The observed seasonal modulation of the urban–rural temperature difference captured in the case of all satellite sensors, emphasises the importance of vegetation dynamics in shaping surface temperature regimes. The progressive rise in NDVI and NDMI during colder months not only improved rural surface moisture retention but also amplified the contrast between vegetated rural zones and heat-retaining urban areas. This led to a clearer and more dominant UHI signal in later datasets, especially in the morning observations where rural cooling was more pronounced. These findings are consistent with the role of vegetation cover and surface wetness as important regulators of land–atmosphere energy exchange, and ultimately, the strength and detectability of UHI effects for semi-arid Mediterranean conditions.

3.3.2. Nighttime Urban–Rural Thermal Contrasts

As shown in Figure 9, the nighttime urban–rural thermal contrast was clearer and more consistent than the daytime case. MODIS indicated persistent urban warming relative to rural areas across all datasets, with urban–rural mean differences typically in the range 0.5–1.6 °C. Prior to bias correction, Sentinel-3 Level-2 data exhibited greater variability, reflecting its moderate spatial resolution and sensitivity to emissivity difference and low-contrast nighttime thermal conditions. After application of the locally adjusted SWA, Sentinel-3 Level-1 results showed a more consistent urban–rural contrast, with urban means frequently being approximately 0.8 °C higher than for rural areas.

The physical mechanisms underlying nocturnal urban warming are well documented. Impervious urban materials (concrete, asphalt, masonry, etc.) possess higher heat capacity and thermal inertia, releasing stored heat after sunset and sustaining elevated surface temperatures. In addition, urban geometry reduces the sky view factor, traps longwave radiation, and suppresses radiative cooling within street canyons and urban notches, further delaying nighttime cooling. Rural areas, particularly those with vegetation or moist soils, typically cool more efficiently due to lower heat storage, greater exposure to the open sky, and the absence of canyon-like structures.

From a methodological perspective, the inherent characteristics of each satellite sensor, such as spatial resolution, spectral response, and retrieval algorithm, played a key role in determining how effectively nocturnal thermal patterns were detected. MODIS, despite its coarse spatial resolution, effectively captured the regional-scale nocturnal urban–rural contrast, as the nighttime signal is spatially extensive and less sensitive to sub-kilometre variability. Sentinel-3 Level-1 SLSTR, processed with a locally tuned SWA at 500 m resolution, reduced the reliance on interpolation and improved consistency with in situ observations. This enabled clearer identification of nocturnal urban–rural temperature differences, broadly consistent with MODIS patterns but with improved spatial detail. However, Landsat-8 does not provide nighttime thermal acquisitions over Malta; therefore, high-resolution nocturnal LST patterns could not be assessed in this case.

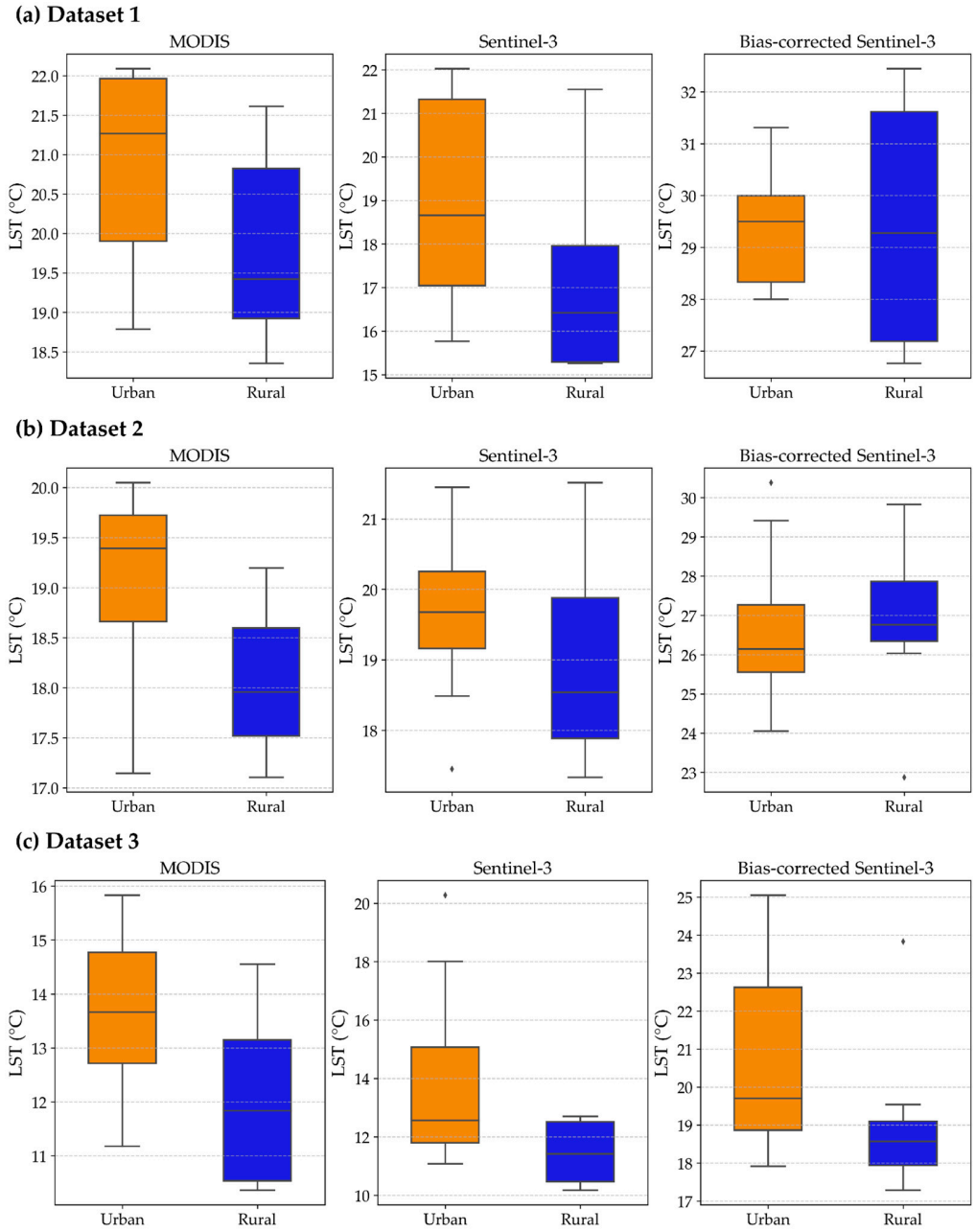


Figure 9. *Cont*.

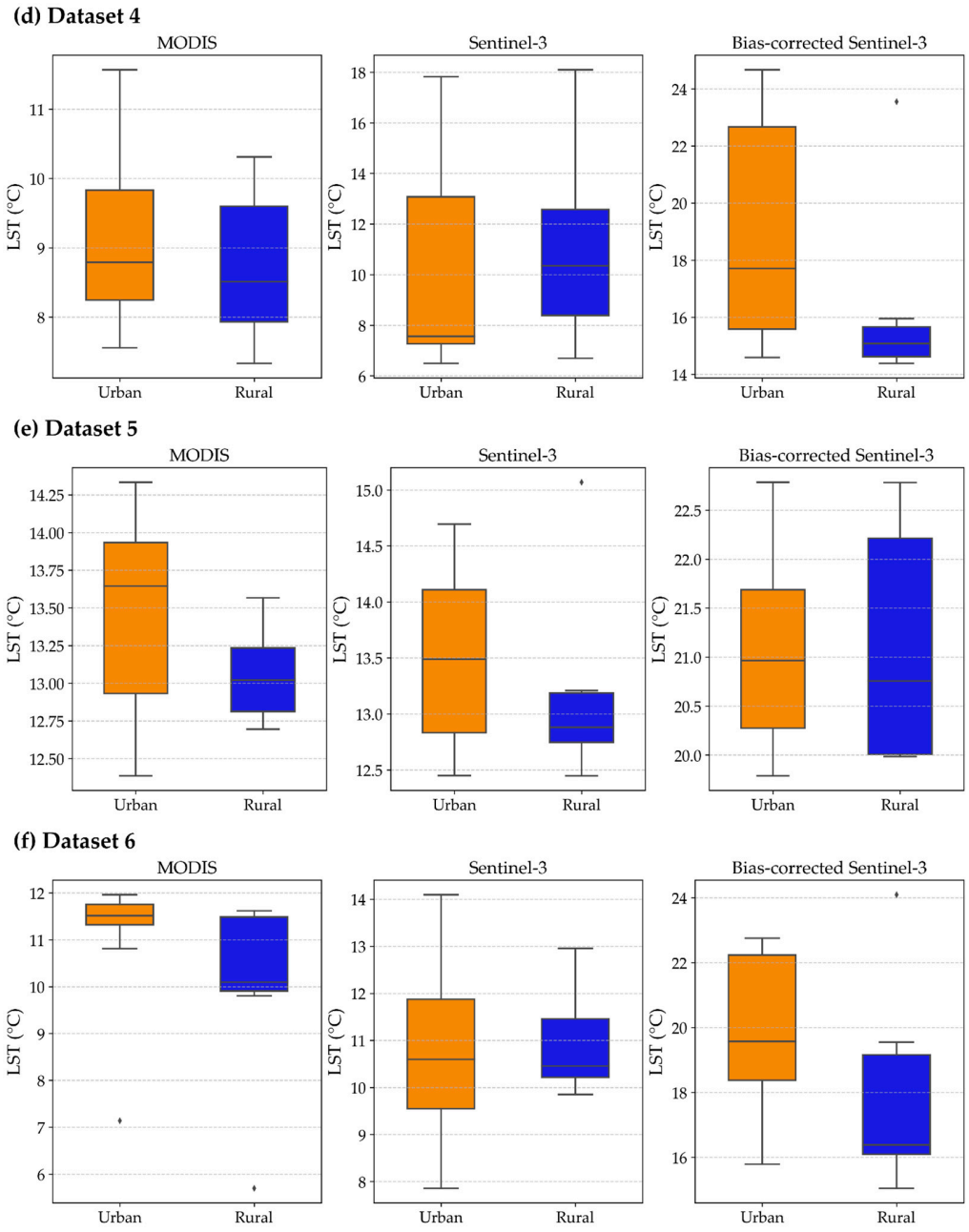


Figure 9. Boxplots showing the distribution of nighttime LST for urban and rural land use classes, derived from MODIS, Sentinel-3 Level-2, and the bias-corrected Sentinel-3 SWA product for each observation day (Datasets 1–6). The boxes represent the IQR, with the horizontal lines within the boxes indicating the median and whiskers extending to 1.5 times the IQR to display variability. The data outliers are points beyond the whiskers. The comparison reveals systematic differences between urban and rural surfaces, with urban areas consistently retaining higher nighttime LST due to greater heat storage capacity and reduced radiative cooling, while rural areas exhibit stronger nocturnal cooling. Variations in the degree of contrast across satellite sensors reflect differences in spatial resolution, retrieval algorithms, and calibration adjustments applied to the Sentinel-3 SWA product.

3.4. Daytime–Nighttime Difference in LST

The analysis of daytime–nighttime differences (DND) in LST between urban and rural environments provides a useful indicator of surface energy exchange, radiative balance, and the influence of thermal inertia in the case of semi-arid Mediterranean climates. Although the datasets do not constitute continuous 24 h measurements, the DND metric, derived from daytime, i.e., morning, and nighttime, i.e., evening, acquisitions, serves

as a practical approximation of sub-diurnal thermal behaviour and enables comparison of surface responses to radiative forcing across different land cover types. As shown in Figure 10a, the in situ NSAT data indicate that rural locations generally experienced greater daytime–nighttime temperature differences than urban locations.

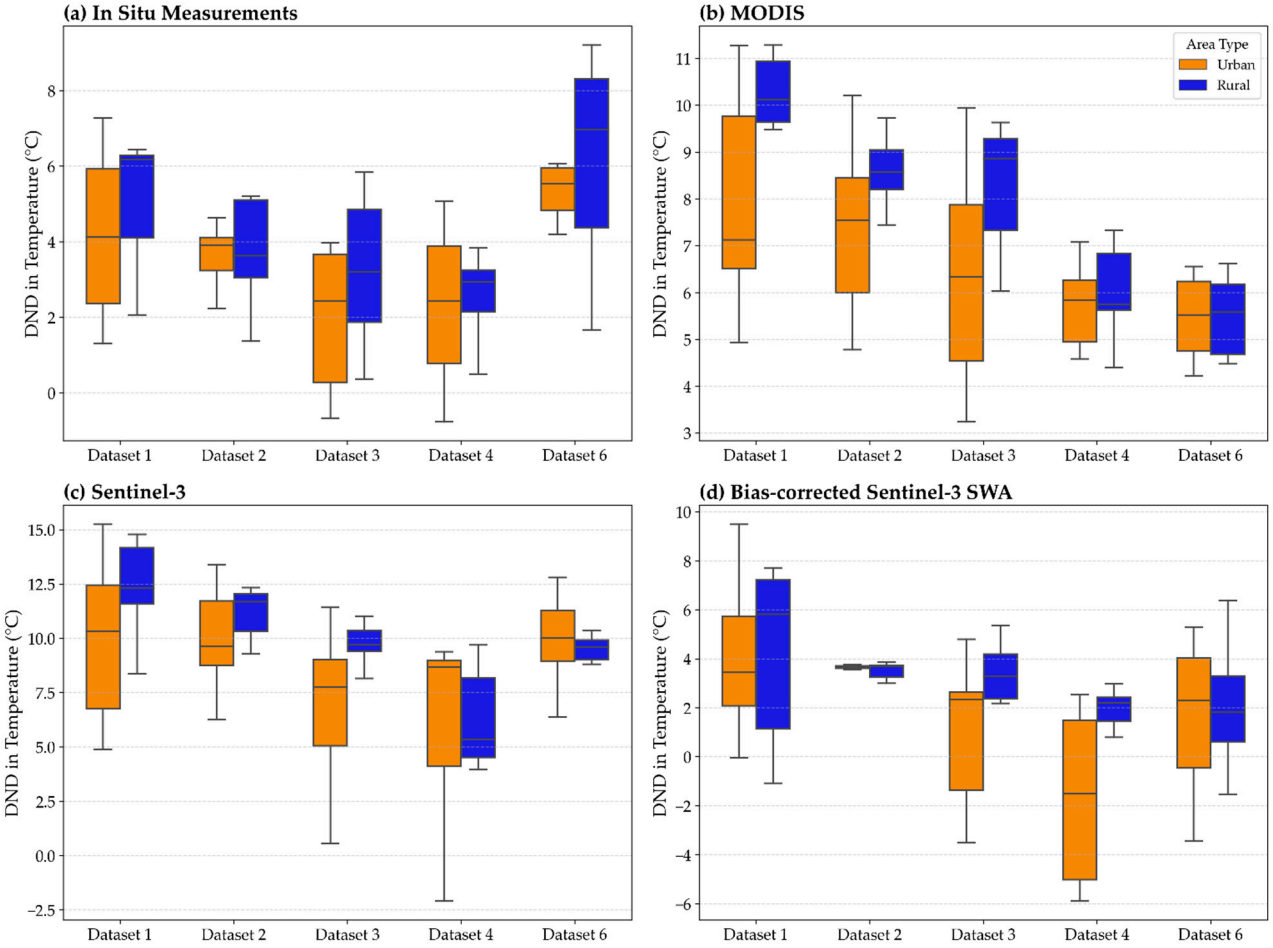


Figure 10. Boxplots illustrating the DND in temperature (LST in the case of satellite data and NSAT for the in situ measurements) for urban and rural areas, for all the datasets, shown separately as follows: (**a**) In situ NSAT measurements, (**b**) MODIS, (**c**) Sentinel-3 Level-2, and (**d**) Bias-corrected Sentinel-3 SWA product. Urban points are represented in orange, and rural points in blue. Each box represents the IQR, with the horizontal lines within the boxes indicating medians, and whiskers extending to 1.5 times the IQR to display variability and outliers. Rural areas generally display greater temperature variability due to lower heat storage capacity and faster nocturnal cooling, whereas urban areas exhibit smaller differences as retained heat within built-up surfaces limits nighttime cooling.

Despite its relatively coarse spatial resolution (~1 km), MODIS captured the generalised class-scale temperature differences between urban and rural areas (refer to Figure 10b). During the warmest observational period, rural areas exhibited median DND values approaching 10.1 °C, compared to 7.5 °C for urban regions.

This behaviour is consistent with established surface energy balance principles. Rural landscapes, typically characterised by exposed soil and vegetation, tend to have lower thermal inertia, allowing them to heat rapidly under solar radiation and cool efficiently through longwave emission after sunset. In contrast, urban materials such as concrete, asphalt, and masonry possess higher thermal mass, storing heat during daytime and releasing it gradually at night, which moderates temperature fluctuations and leads to smaller DND values.

The Sentinel-3 Level-2 product (refer to Figure 10c), which also operates at 1 km resolution, displayed a broader range of DND variability. In some datasets, rural areas maintained distinctly higher DND than urban areas (e.g., 12.5 °C for rural vs. 10.5 °C for urban areas), while in others, the differences were negligible or even inverted.

This variability is likely influenced by mixed-pixel effects, residual atmospheric contributions, and the use of interpolation techniques such as IDW to relate coarse satellite pixels to the sampling points. These processes may smooth out or obscure local thermal extremes and alter the apparent magnitude of the DND.

The bias-corrected Sentinel-3 SWA product (refer to Figure 10d), with its effective spatial resolution of 500 m, showed generally reduced DND values, often around 4 °C, particularly in urban areas. In several cases, the median urban DND approached zero or became slightly negative, indicating situations where nighttime LST exceeded morning values. This behaviour is consistent with the combined effects of urban heat retention and the harmonisation procedure applied to the Sentinel-3 data, which tends to moderate extreme daytime values. Rural sites, by contrast, continued to exhibit more pronounced DND values (e.g., 4.5 °C for rural versus 2.0 °C for urban), consistent with more efficient radiative cooling and lower heat storage capacity.

From a physical standpoint, the generally higher DND in LST that is observed in rural environments can be associated with several factors. Firstly, the low thermal inertia of soils and vegetation allows for rapid temperature response to incoming and outgoing radiative fluxes. Secondly, radiative cooling efficiency is higher in rural areas due to their elevated surface emissivity and unobstructed sky view, which generally facilitate more efficient longwave radiation loss during nighttime. Thirdly, the absence of anthropogenic heat sources, such as building emissions, vehicular activity, and energy consumption reduces the residual heat flux after sunset. Finally, rural regions lack the complex geometry of urban street canyons, which tend to trap outgoing radiation and limit convective heat dissipation, thereby further amplifying the DND in LST.

In summary, although the analysis does not represent a continuous 24 h cycle, the DND metric provides a useful indicator of sub-diurnal surface thermal behaviour across various land cover types. MODIS captured broad class-scale contrasts, while Sentinel-3, particularly the bias-corrected SWA product, offered improved spatial detail and sensitivity to local variability. Overall, the results suggest that rural areas tend to exhibit larger temperature amplitudes, whereas urban areas show more moderated daytime–nighttime differences due to heat storage and urban geometry. These patterns are broadly consistent with established urban–rural thermal behaviour in semi-arid Mediterranean environments, within the limitations of the observational framework.

4. Discussion

This study presents a comparative analysis of satellite-derived LST products over Malta, using observations from Landsat-8, MODIS, and Sentinel-3 (both Level-2 and bias-corrected Level-1), in conjunction with ground-based in situ NSAT measurements (as a surrogate to LST). The analysis focuses on the consistency between satellite-derived LST and near-surface atmospheric conditions, rather than on strict validation of radiometric LST accuracy. The results provide insight into spatial and temporal thermal behaviour across urban and rural land types, seasonal transitions, and morning–night contrasts, with particular reference to the manifestation of the urban heat island (UHI) effect in a semi-arid Mediterranean island environment.

The daytime (morning) analyses reveal a seasonal modulation of the classical UHI signature. During the warmer part of the observational period (late summer and early autumn), rural areas exhibited higher satellite-derived surface temperatures than urban

zones. This pattern was especially evident in the September and October datasets, when limited vegetation cover and low surface moisture in rural areas promoted rapid solar heating of exposed soils. Such surfaces respond quickly to incoming radiation due to their relatively low thermal inertia, leading to elevated morning LST values. In contrast, urban environments, despite their impervious materials, are influenced by shading, complex geometry, and reflective surfaces, which can moderate early morning warming.

Conversely, in the cooler months, a shift in the thermal landscape is observed. The recovery of vegetative cover in rural areas, confirmed by increasing NDVI and NDMI values derived from Sentinel-2, contributes to enhanced evapotranspiration and soil moisture retention. These processes substantially reduce rural daytime temperatures, re-establishing the expected urban–rural temperature difference indicative of the UHI phenomenon. The seasonal modulation of the UHI effect, rather than its persistent presence, aligns with similar findings in other semi-arid regions, where vegetation dynamics strongly influence surface energy partitioning.

Nighttime analyses revealed a more consistent urban–rural temperature difference. MODIS and Sentinel-3 products both indicated persistent nocturnal urban warming across all observational periods. This pattern aligns with well-established physical mechanisms; impervious urban materials possess higher thermal inertia and release stored heat after sunset, while reduced sky view factors in urban canyons inhibit radiative cooling. Rural areas, particularly those with vegetation or moist soils, cool more efficiently due to lower heat storage and greater exposure to the open sky. The persistence of nocturnal urban warming, even in a small island setting, highlights the diagnostic value of nighttime thermal observations under clear-sky conditions.

The performance of Sentinel-3 illustrates the sensitivity of moderate-resolution thermal retrievals to local atmospheric and surface conditions. The native Level-2 product exhibited variable results, with notable inconsistencies in both daytime and nighttime LST retrievals. This is likely due to mixed pixels, coastal influences, and atmospheric uncertainties. After applying a locally adjusted split-window algorithm, the Sentinel-3 Level-1 product showed improved consistency with NSAT observations and with the broader spatial patterns observed in MODIS. However, the adjustment effectively harmonises satellite-derived LST with NSAT rather than producing a purely radiometric LST product. Residual anomalies, such as reduced daytime–nighttime temperature amplitudes in some urban areas, indicate that further refinement of local calibration parameters may be necessary for small island environments.

Analysis of morning–night temperature differences further highlights the role of surface thermal inertia. Rural areas consistently exhibited larger temperature ranges, reflecting rapid heating during the morning and efficient radiative cooling during nighttime. Urban surfaces showed more moderate temperature amplitudes, consistent with greater heat storage and delayed nocturnal cooling. These patterns were evident in both satellite-derived LST and in situ NSAT datasets, although moderate-resolution products were more affected by mixed-pixel effects and calibration adjustments.

This study highlights the challenge posed by resolution mismatches between that of satellite sensors and local-scale urban features. MODIS, despite its coarse spatial resolution, effectively captured broad urban–rural contrasts when results were aggregated by land cover class. However, its inability to resolve finer intra-urban heterogeneity necessitated the use of IDW interpolation to enable spatial comparisons with point-based in situ measurements. Landsat-8, with its higher spatial resolution, provided more detailed representations of local thermal variability but was limited by its low revisit frequency and lack of nighttime acquisitions. The bias-corrected Sentinel-3 Level-1 product offered

an intermediate solution, combining moderate spatial detail with regular revisit intervals, although its performance remains dependent on local calibration.

These findings have practical implications for thermal monitoring in semi-arid island environments. The results indicate that nighttime satellite observations provide more stable indicators of urban–rural thermal contrasts, particularly under clear-sky conditions. Moderate-resolution sensors such as MODIS and Sentinel-3 are effective for capturing class-scale UHI behaviour when interpreted at appropriate spatial scales, while higher-resolution platforms such as Landsat-8 remain essential for resolving local thermal variability within urban environments. Together, these observations highlight the importance of selecting satellite products according to the spatial scale and temporal frequency required for specific urban climate applications.

Limitations and Future Directions

This study is subject to several limitations that should be considered when interpreting the results. For instance, the observational period spans only six months, from September to February, and does not include the core summer season. As a result, the analysis does not capture peak heat stress conditions or the full annual cycle of UHI behaviour. Consequently, the seasonal patterns described here apply primarily to late summer, autumn, and winter conditions.

Furthermore, the in situ measurements were collected during discrete monthly campaigns rather than as continuous time series. Exact temporal matching with satellite overpasses was not always possible, and comparisons were therefore performed under comparable synoptic conditions rather than strict time coincidence. An additional consideration concerns the relatively limited sample size of the in situ dataset. The analysis is based on data from 19 monitoring sites collected during six monthly campaigns, which, when subdivided by land cover class, sensor, and acquisition period, results in relatively small sample groups. This reduces the statistical effectiveness of formal significance tests and increases sensitivity to local variability and representativeness effects. Consequently, the reported correlations, biases, and urban–rural contrasts should be interpreted as indicative of class-scale thermal tendencies rather than precise point-scale validations. Despite this limitation, the consistency of the main patterns for the considered satellite sensors, observation periods, and land cover classes suggests that the identified seasonal and nocturnal thermal behaviours are robust at the scale of analysis adopted in this study.

The study compares point-based NSAT measurements with data pertaining to satellite pixels ranging from 30 m to 1 km in size. Especially for coarse-resolution sensors, these pixels represent mixed land cover types, introducing representativeness errors that cannot be fully eliminated through interpolation. Consequently, the results should be interpreted as site-representative at class-scale levels rather than as exact point-to-pixel validations.

Finally, the empirical calibration applied to Sentinel-3 Level-1 data harmonises satellite-derived LST with NSAT measurements. While this improves consistency for comparative analysis, it does not necessarily represent a physically corrected radiometric LST product.

Future work should extend the observational period to cover a full annual cycle, including peak summer conditions, and incorporate continuous in situ monitoring where feasible. The inclusion of direct radiometric LST measurements would also allow more rigorous validation of satellite-derived LST products. Such improvements would enhance the robustness of thermal monitoring frameworks for small island and coastal environments.

5. Conclusions

This study examined the relationship between satellite-derived LST and in situ NSAT across Malta using observations from Landsat-8, MODIS, and Sentinel-3. Rather than treat-

ing the in situ measurements as direct validation of radiometric LST, the analysis focused on the consistency between satellite-derived surface temperatures and local atmospheric thermal conditions across different land cover classes and observation periods.

At this point, it should be emphasised that at least an element of deviation between in situ measurements and satellite data products is due to the fact that the former measures NSAT and not LST. Essentially, the said deviation could, in part, reflect the comparison of two inherently distinct physical quantities.

The results indicate that Landsat-8 provided the strongest spatial correspondence with in situ NSAT, reflecting its higher spatial resolution and improved sensitivity to local thermal contrasts. MODIS, despite its coarse spatial resolution, captured consistent class-scale thermal patterns and temporal behaviour across the study period. Sentinel-3 Level-2 products showed larger differences relative to NSAT, particularly at night; however, the locally adjusted split-window approach improved consistency with in situ observations and enhanced the detection of urban–rural contrasts at moderate spatial scales.

Across all datasets, rural areas generally exhibited larger day–night temperature differences, while urban areas retained heat more effectively, especially under nighttime conditions. Nevertheless, the magnitude and, in some cases, the direction of the urban–rural contrast varied seasonally, reflecting changes in vegetation cover and surface moisture. During the drier months, rural areas occasionally displayed higher morning LST, whereas in the cooler months, the more typical urban warming signal became more pronounced.

These findings are broadly consistent with previous studies on satellite-derived LST and urban thermal behaviour. Earlier work has shown that coarse-resolution sensors such as MODIS effectively capture regional-scale UHI patterns but tend to smooth out local heterogeneity, while higher-resolution platforms such as Landsat are better suited for resolving fine-scale urban thermal contrasts [1,2,36,45]. Similar to the outcomes from this work, validation studies have reported systematic differences between satellite-derived LST and NSAT, particularly under humid or heterogeneous surface conditions [24,25]. The improved consistency achieved through local calibration of the Sentinel-3 product also aligns with recent studies emphasising the importance of region-specific parameterisation and data-driven correction approaches for accurate surface temperature retrievals [26–28,37].

Overall, the study demonstrates that multi-sensor analysis can provide useful insights into class-scale thermal behaviour in the case of small island environments, provided that differences in spatial resolution, observation timing, and the physical distinction between LST and NSAT are carefully considered. The results highlight the importance of scale-aware interpretation and, where appropriate, local adjustment of satellite products when applied to thermally heterogeneous landscapes.

For long-term thermal monitoring in small island environments such as Malta, a multi-sensor approach is recommended. Moderate-resolution sensors such as MODIS and Sentinel-3 provide frequent daytime and nighttime observations that are well suited for continuous, class-scale monitoring of urban–rural thermal behaviour. High-resolution platforms such as Landsat-8, although limited in terms of revisit frequency, remain essential for resolving fine-scale intra-urban temperature patterns and identifying localised heat stress hotspots. Therefore, the combined use of frequent moderate-resolution data and periodic high-resolution observations represents the most effective strategy for long-term LST monitoring in small, heterogeneous island settings.

Author Contributions: Conceptualisation, A.G. and A.M.; methodology, D.W., A.G., and A.M.; software, D.W.; validation, D.W., A.G., and A.M.; formal analysis, D.W.; investigation, D.W., A.G., and A.M.; resources, D.W., A.G., and A.M.; data curation, D.W.; writing—original draft preparation, D.W.; writing—review and editing, D.W., A.G., and A.M.; visualisation, D.W.; supervision, A.G. and A.M. All authors have read and agreed to the published version of the manuscript.

Funding: This research received no external funding. All funding was provided by the University of Malta.

Data Availability Statement: All datasets and computer code associated with this study will be made available upon request.

Conflicts of Interest: The authors declare no conflicts of interest.

References

1. Li, Z.-L.; Tang, B.-H.; Wu, H.; Ren, H.; Yan, G.; Wan, Z.; Trigo, I.F.; Sobrino, J.A. Satellite-derived land surface temperature: Current status and perspectives. *Remote Sens. Environ.* **2013**, *131*, 14–37. [CrossRef]
2. Zhou, D.; Xiao, J.; Bonafoni, S.; Berger, C.; Deilami, K.; Zhou, Y.; Frolking, S.; Yao, R.; Qiao, Z.; Sobrino, J.A. Satellite remote sensing of surface urban heat islands: Progress, challenges, and perspectives. *Remote Sens.* **2018**, *11*, 48. [CrossRef]
3. Oke, T.R. The energetic basis of the urban heat island. *Bound.-Layer Meteorol.* **1982**, *24*, 1–24. [CrossRef]
4. Carlson, T.N.; Dodd, J.K.; Benjamin, S.G.; Cooper, J.N. Satellite estimation of the surface energy balance, moisture availability and thermal inertia. *J. Appl. Meteorol.* **1981**, *20*, 67–87. [CrossRef]
5. Trenberth, K.E.; Fasullo, J.T.; Kiehl, J. Earth's global energy budget. *Bull. Am. Meteorol. Soc.* **2009**, *90*, 311–324. [CrossRef]
6. Bou-Zeid, E.; Anderson, W.; Katul, G.G.; Mahrt, L. The persistent challenge of surface heterogeneity in boundary-layer meteorology: A review. *Bound.-Layer Meteorol.* **2020**, *177*, 227–245. [CrossRef]
7. Lu, L.; Weng, Q.; Xiao, D.; Guo, H.; Li, Q.; Hui, W. Spatiotemporal variation of surface urban heat islands in relation to land cover composition and configuration. *Remote Sens.* **2020**, *12*, 2713. [CrossRef]
8. Hottel, H.C. A simple model for estimating the transmittance of direct solar radiation through clear atmospheres. *Sol. Energy* **1976**, *18*, 129–134. [CrossRef]
9. Wu, W.; Liu, Y. Radiation entropy flux and entropy production of the Earth system. *Rev. Geophys.* **2010**, *48*, RG2003. [CrossRef]
10. Reuter, D.C.; Richardson, C.M.; Pellerano, F.A.; Irons, J.R.; Allen, R.G.; Anderson, M.; Jhabvala, M.D.; Lunsford, A.W.; Montanaro, M.; Smith, R.L.; et al. The thermal infrared sensor (TIRS) on Landsat 8: Design overview and pre-launch characterization. *Remote Sens.* **2015**, *7*, 1135–1153. [CrossRef]
11. Williams, D.L.; Goward, S.; Arvidson, T. Landsat: Yesterday, today, and tomorrow. *Photogramm. Eng. Remote Sens.* **2006**, *72*, 1171–1178. [CrossRef]
12. Montanaro, M.; McCorkel, J.; Tveekrem, J.; Stauder, J.; Mentzell, E.; Lunsford, A.; Hair, J.; Reuter, D. Landsat 9 thermal infrared sensor 2 (TIRS-2) stray light mitigation and assessment. *IEEE Trans. Geosci. Remote Sens.* **2022**, *60*, 5002408. [CrossRef]
13. Pagano, T.S.; Durham, R.M. Moderate resolution imaging spectroradiometer (MODIS). In *Sensor Systems for the Early Earth Observing System Platforms*; SPIE: Bellingham, WA, USA, 1993; Volume 1939, pp. 2–17.
14. Donlon, C.; Berruti, B.; Buongiorno, A.; Ferreira, M.-H.; Féménias, P.; Frerick, J.; Goryl, P.; Klein, U.; Laur, H.; Mavrocordatos, C.; et al. The global monitoring for environment and security (GMES) Sentinel-3 mission. *Remote Sens. Environ.* **2012**, *120*, 37–57. [CrossRef]
15. Wan, Z.; Dozier, J. A generalized split-window algorithm for retrieving land-surface temperature from space. *IEEE Trans. Geosci. Remote Sens.* **1996**, *34*, 892–905.
16. Sobrino, J.A.; Jiménez-Muñoz, J.C.; Paolini, L. Land surface temperature retrieval from LANDSAT TM 5. *Remote Sens. Environ.* **2004**, *90*, 434–440. [CrossRef]
17. Gerace, A.; Kleynhans, T.; Eon, R.; Montanaro, M. Towards an operational split-window surface temperature product for the thermal infrared sensors onboard Landsat 8 and 9. *Remote Sens.* **2020**, *12*, 224. [CrossRef]
18. Barnes, W.L.; Pagano, T.S.; Salomonson, V.V. Prelaunch characteristics of the moderate resolution imaging spectroradiometer (MODIS) on EOS-AM1. *IEEE Trans. Geosci. Remote Sens.* **1998**, *36*, 1088–1100. [CrossRef]
19. Coppo, P.; Smith, D.; Nieke, J. Sea and land surface temperature radiometer on Sentinel-3. In *Optical Payloads for Space Missions*; Wiley: Hoboken, NJ, USA, 2015; pp. 701–714.
20. Smith, D.; Barillot, M.; Bianchi, S.; Brandani, F.; Coppo, P.; Etxaluze, M.; Frerick, J.; Kirschstein, S.; Lee, A.; Maddison, B.; et al. Sentinel-3A/B SLSTR pre-launch calibration of the thermal infrared channels. *Remote Sens.* **2020**, *12*, 2510. [CrossRef]
21. Hook, S.J.; Myers, J.J.; Thome, K.J.; Fitzgerald, M.; Kahle, A.B. The MODIS/ASTER airborne simulator (MASTER): A new instrument for Earth science studies. *Remote Sens. Environ.* **2001**, *76*, 93–102. [CrossRef]
22. El Kenawy, A.M.; Hereher, M.E.; Robaa, S.M. An assessment of the accuracy of MODIS land surface temperature over Egypt using ground-based measurements. *Remote Sens.* **2019**, *11*, 2369. [CrossRef]
23. Li, Z.-L.; Wu, H.; Duan, S.-B.; Zhao, W.; Ren, H.; Liu, X.; Leng, P.; Tang, R.; Ye, X.; Zhu, J.; et al. Satellite remote sensing of global land surface temperature: Definition, methods, products, and applications. *Rev. Geophys.* **2023**, *61*, e2022RG000787. [CrossRef]
24. Dyukarev, E.; Voropay, N.; Vasilenko, O.; Rasputina, E. Validation of remotely sensed land surface temperature at Lake Baikal's surroundings using in situ observations. *Land* **2024**, *13*, 555. [CrossRef]

25. Ermida, S.L.; Trigo, I.F.; DaCamara, C.C.; Göttsche, F.M.; Olesen, F.S.; Hulley, G. Validation of remotely sensed surface temperature over an oak woodland landscape. *Remote Sens. Environ.* **2014**, *148*, 16–27. [CrossRef]
26. Wang, S.; Zhou, J.; Lei, T.; Wu, H.; Zhang, X.; Ma, J.; Zhong, H. Estimating land surface temperature from satellite passive microwave observations using neural networks. *Remote Sens.* **2020**, *12*, 2691. [CrossRef]
27. Xu, C.; Lin, M.; Fang, Q.; Chen, J.; Yue, Q.; Xia, J. Air temperature estimation over winter wheat fields using machine learning and remote sensing. *Int. J. Appl. Earth Obs. Geoinf.* **2023**, *122*, 103416.
28. Lee, S.; Yoo, C.; Im, J.; Cho, D.; Lee, Y.; Bae, D. A hybrid machine learning approach to investigate urban thermal environment changes. *Int. J. Appl. Earth Obs. Geoinf.* **2023**, *122*, 103408.
29. Agathangelidis, I.; Cartalis, C.; Polydoros, A.; Mavrakou, T.; Philippopoulos, K. Can satellite-based thermal anomalies indicate heatwaves? *Remote Sens.* **2022**, *14*, 3139. [CrossRef]
30. Ermida, S.L.; Soares, P.M.M.; Mantas, V.; Göttsche, F.M.; Trigo, I.F. Google Earth Engine open-source code for land surface temperature estimation from the Landsat series. *Remote Sens.* **2020**, *12*, 1471. [CrossRef]
31. Zhan, W.; Chen, Y.; Zhou, J.; Wang, J.; Liu, W.; Voogt, J.A.; Zhu, X.; Quan, J.; Li, J. Disaggregation of remotely sensed land surface temperature: Literature survey, taxonomy, issues, and caveats. *Remote Sens. Environ.* **2013**, *131*, 119–139. [CrossRef]
32. Concejal, A. Measuring moisture: Normalized Difference Moisture Index (NDMI) Sentinel-2. Available online: https://geovisualization.net/2022/07/14/measuring-moisture-normalized-difference-moisture-index-ndmi-sentinel-2-2022/ (accessed on 14 July 2022).
33. Parkside. Parkside PKDL A1 Temperature and Humidity Monitor User Manual, 2023. Available online: https://manuals.plus/parkside/ian376306_2104-temperature-and-humidity-monitor-manual (accessed on 23 April 2025).
34. AMES. Handheld Anemometer RVM 96B-1 User Manual, 2011. Available online: https://www.ames.si/files/attachments/RVM96B_1_broch_rev3.pdf (accessed on 7 March 2025).
35. Hulley, G.C.; Hook, S.J.; Baldridge, A.M. Investigating the effects of soil moisture on thermal infrared land surface temperature retrievals. *Remote Sens. Environ.* **2014**, *149*, 204–216.
36. Voogt, J.A.; Oke, T.R. Thermal remote sensing of urban climates. *Remote Sens. Environ.* **2003**, *86*, 370–384. [CrossRef]
37. Ma, Y.; Wang, S.; Zhang, L.; Wang, S.; Liang, S.; Li, X. Review of satellite-based land surface temperature retrieval methods. *ISPRS J. Photogramm. Remote Sens.* **2021**, *175*, 1–21.
38. Peng, S.; Piao, S.; Zeng, Z.; Ciais, P.; Zhou, L.; Li, L.Z.X.; Myneni, R.B.; Yin, Y.; Zeng, H. Afforestation in China cools local land surface temperature. *Proc. Natl. Acad. Sci. USA* **2014**, *111*, 2915–2919.
39. Zanaga, D.; Van De Kerchove, R.; De Keersmaecker, W.; Souverijns, N.; Brockmann, C.; Quast, R.; Wevers, J.; Grosu, A.; Paccini, A.; Vergnaud, S.; et al. ESA WorldCover 10 m 2021 v200. *Zenodo* **2022**. [CrossRef]
40. Badarinath, K.V.S.; Chand, T.R.K.; Madhavilatha, K.; Raghavaswamy, V. Studies on urban heat islands using AATSR data. *J. Indian Soc. Remote Sens.* **2005**, *33*, 495–501. [CrossRef]
41. Oke, T.R. *Boundary Layer Climates*, 2nd ed.; Routledge: London, UK, 1987.
42. Stewart, I.D.; Oke, T.R. Local climate zones for urban temperature studies. *Bull. Am. Meteorol. Soc.* **2012**, *93*, 1879–1900. [CrossRef]
43. Han, D.; Zhang, T.; Qin, Y.; Tan, Y.; Liu, J. A comparative review of UHI mitigation strategies. *Clim. Dev.* **2023**, *15*, 379–403. [CrossRef]
44. Boujelbene, M.; Boukholda, I.; Guesmi, T.; Amara, M.B.; Khalilpoor, N. Solar reflection and effect of roof surfaces material characteristics in heat island mitigation: Toward green building and urban sustainability in Ha'il, Saudi Arabia. *Int. J. Low-Carbon Technol.* **2023**, *18*, 1039–1047. [CrossRef]
45. Weng, Q.; Lu, D.; Schubring, J. Estimation of land surface temperature–vegetation abundance relationship for urban heat island studies. *Remote Sens. Environ.* **2004**, *89*, 467–483.

Disclaimer/Publisher's Note: The statements, opinions and data contained in all publications are solely those of the individual author(s) and contributor(s) and not of MDPI and/or the editor(s). MDPI and/or the editor(s) disclaim responsibility for any injury to people or property resulting from any ideas, methods, instructions or products referred to in the content.